Draft for Review
Not for Publication

FABRICATION AND TESTING OF MAINTENANCE EQUIPMENT USED FOR PAVEMENT SURFACE REPAIRS

Final Report of Phase II - Part II

SHRP H-107A

Participating Organizations
University of California, Davis
California Department of Transportation
Bechtel, Inc.
ERES Consultants, Inc.

Steven A. Velinsky, Principal Investigator
Department of Mechanical Engineering
University of California, Davis

July 31, 1992

Strategic Highway Research Program
National Research Council
Washington, D.C.

TABLE OF CONTENTS

LIST OF FIGURES

LIST OF TABLES

1.0 - TESTING OF FIRST GENERATION COMPONENT PROTOTYPES

1.1 - Introduction

The ultimate goal of the SHRP H-107A project is to develop prototype automated machinery that will sense, prepare, and seal (or fill) cracks and joints on pavement. As such, the primary objectives of this project are to design machinery for the sealing and filling of joints and cracks in pavement in order to:

- Increase the cost-effectiveness of these operations,
- Increase the quality, consistency, and life of the resultant seals and fills,
- Increase the safety of workers and highway users, and
- Increase the use of remote operation and control of equipment to attain the above.

Machinery that satisfies these objectives will additionally reduce lane and highway closures and thus, will play a significant role in reducing traffic congestion, an area of considerable concern in the major urban regions around the world. The cost effectiveness of such machinery is due to a combination of the increased speed of sealing and reduced manpower needs, in addition to the higher quality seal which will reduce the frequency of major highway rehabilitations.

In order to have the greatest impact, such machinery should satisfactorily perform the following functions automatically:

- Sense the occurrence and location of cracks in pavement.
- Adequately prepare the pavement surface for sealing/filling with the appropriate methods; for example, any operation that is deemed necessary such as removing entrapped moisture and debris, preheating the road to ensure maximum sealant adhesion, refacing of reservoirs, etc.
- Prepare the sealant/filler for application; i.e., heat and mix the material, etc.
- Dispense the sealant/filler.
- Form the sealer/filler into the desired configuration.
- Finish the sealer/filler.

Additionally, as overall functional specifications, this machinery should be:

- Reasonable in cost,
- Easy to use,
- Reliable and fast,

- Rugged,
- Safe,
- Capable of being driven on the highway under its own power,
- Self-contained (contain all of the components necessary to perform task),
- Primarily powered by an internal combustion engine,
- Provided with a heavy duty electrical system with sufficient capacity for safe operation of all components,
- Compatible with repair materials to be identified under SHRP H-106,
- Fabricated in such a manner that the eventual addition of safety lighting & appurtenances (arrow boards, etc.) is possible, and
- Compliant with any applicable OSHA standards.

Phase I of this project involved a feasibility study on the possible development of the automated pavement repair machinery discussed above, the design of first generation machine components, and the conceptual design of the integrated prototype machinery. Phase I work was performed during the period December 1, 1990 through May 31, 1991. A detailed report discussing these items was delivered at the end of Phase I, the Phase I Final Report, at which time continuation through Phase II was approved.

Phase II of the H-107A project included two specific tasks; TASK 3) the fabrication of first generation component prototypes, and TASK 4) the testing of these components and the development of component modifications based on this testing. More globally, the goal of this phase was to make satisfactory progress concerning machine components such that the development of the integrated machinery in the last phase can be accomplished. Phase II work was performed during the period from June 1, 1991 through March 31, 1992.

1.2 - Purpose

The purpose of this document, Part II of the Phase II Final Report, is to report on the completion of TASK 4 of SHRP H107A, Conduct a Laboratory Test Program Using Prototype Components & Prepare an Interim Report of Phase II. This task involved the design of test plans for the components, the development of required test software and hardware including test apparatus, the performance of testing, and the analysis of results. This testing has been carried out with the first generation components of the SHRP H-107A project. Detailed descriptions of the design and fabrication of the first generation components is discussed in Part I of the Phase II Final Report which concerns TASK 3 of SHRP H-107A, Fabrication of First Generation Prototypes.

In the sections that follow, detailed component subsystem testing and results is discussed. The machine subsystem descriptions and their functions have been discussed in numerous previous SHRP H-107A reports, and the same nomenclature is utilized herein. The Integration and Control Unit (ICU) is discussed first, in Section 2, followed by the Vision Sensing and Local Sensing Systems (VSS and LSS) in Sections 3 and 4, respectively. The remaining three sections cover the Robot Positioning System (RPS), Applicator and Peripherals System (APS), and Vehicle Orientation and Control System (VOC).

The remainder of the H-107A project involves the development of the prototype integrated machinery, its field testing, and the reporting of results and documentation. These activities are comprised in Phases III and IV which are divided into four tasks. Since SHRP's sunset is March 31, 1993, the H-107A project must be entirely completed by that date. Accordingly, Phases III and IV encompass 12 months.

2.0 - INTEGRATION AND CONTROL UNIT (ICU)

2.1 - Introduction

The development of an Automated Crack Sealing machine (ACSM) includes the integration of a variety of sensing, command and actuating systems, many of which will synchronously perform tasks in real-time. A control architecture has been developed to assure that these systems act in a coordinated manner to achieve the overall goal of sealing pavement cracks at an acceptable performance level. The Integration and Control Unit (ICU) of the Automated Crack Sealing Machine oversees all operations from start to finish. The overall function of the ICU is to coordinate the operations of the automated crack sealing machine, provide the necessary means for information flow between the separate operations, and to otherwise oversee the machine's operation. The ICU test plan developed for Phase II will be used to test the control and communication capabilities of the ICU. In particular, the tests will show that the ICU can recognize input and affect an appropriate machine response with its input.

With respect to its requirements, the ICU must be able to communicate with other sub-systems via a standardized communications protocol. It should accept sensor information from a variety of standard sensor inputs and provide digital and analog control information. In addition to the above it should provide a user interface which is capable of using control information given by the user and providing feedback to the user both auditory and visual. It should be capable of performing self diagnostics on all of its hardware. In review of the machine description in the Phase I report, it is necessary for the ICU to meet the following functional requirements:

- fast and efficient computation
- able to recognize and process prioritized interrupts
- process concurrent information rapidly (multi-tasking).

In the subsections to follow, details of a series of tests that were performed on the ICU during Phase II are presented.

2.2 - Experimental Method

2.2.1 - Test 1: Acceptance Testing of the Delivered Hardware

Upon delivery of the specified ICU hardware each of the components were configured and tested for specified functionality. The components specified and received are (please see the Phase II, Part I Report for a complete, descriptive list):

Backplane (HSE/17R-12V-W60-F3-S150-Ethernet Cables)

- used to house the system boards and bus

CPU Card (HK68H/V3E-4MB)

Analog I/O Card (XVME540)

- used for I/O from/to such components as temperature and pressure sensors

Digital I/O Card (XVME201)

- used for I/O from/to such components as discrete state elements

Communications Card (CMC ENP-10)

- used for Ethernet communications between the ICU and other intelligent subsystems such as the Vision System (VSS) and the Robot System (RPS)

Multi Media Graphics Card (MMI250)

- used for user interface graphics

Setup: Input/Output ports have several different modes of operation and options within those modes; these must be precisely set by sending certain codes to the control registers. The programming team developed configuration and initialization procedures to clear control registers and set up the ports for their intended use. ICU input/output boards were set to accept and place information on the 'correct' lines using a standard format. The configuration routines for the ICU boards reside in several independent routines: analogio.c or anrave.c, diotimer.c, demo540.c, proc1.c, and system.c. These routines specifically initialize and diagnose the XVME540 (Analog I/O), XVME201 (Digital I/O), and HK68H/V3E-4MB (CPU) boards of the ICU.

Procedure: Specification sheets for each board were examined and the desired control register contents were determined. Board configuration and acceptance was executed one board at a time. For each board, a routine was written in 'C' code that configures and initialized the board. A basic logic analyzer device (breakout box showing which lines are high and which are low using LEDs and ribbon cable attachments) was used to detect logic problems.

2.2.2 - Test 2: Data Communications with Other ACSM Subsystems

The task of communicating with ACSM subsystem refers to Ethernet communications through the ENP10 Ethernet board and backbone. Ethernet communication will be used with sub-systems such as the Vision Sensing System and the Robot Positioning System. At this point in the project, the vision system information passing is simulated through the Sun workstation. Communication from the workstation to the ICU is via the Ethernet. Data from the vision system is sent over the Ethernet network to the ICU. The ICU waits for the data and displays it on the user interface whenever it is transmitted. The ICU displays a window once a data transmission begins and closes it after data transmission is complete. The socket.c, comdraw.c, drawarray.c, hold.c, and send.c routines facilitate the task of communication over the CMC ENP-10 (Ethernet) board.

Set-up: The sub-system chosen was the Vision Sensing System (VSS). This sub-systems was simulated on a Sun workstation. Connection to the ICU was via Ethernet. Software was developed on both the ICU and the workstation to facilitate the flow of "crack" information. Figure 2.1 shows the setup described above.

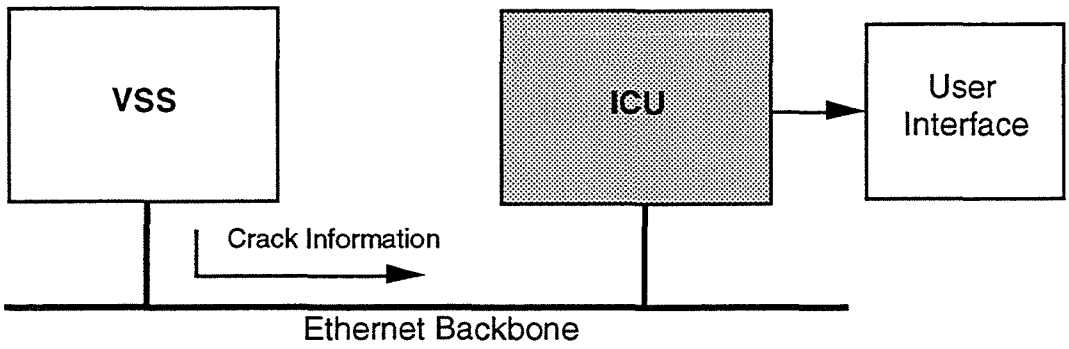

Figure 2.1 *- Experimental Set-up for ICU Test 2.*

Procedure: Crack information from the VSS was recorded on a disk and transfered to the Sun workstation. A communication path with the ICU is established by the VSS. Information is sent by the VSS over the Ethernet to the ICU. ICU displays this information on the user interface by popping up a display window.

2.2.3 - Test 3: Input/Output Interfacing with Test Hardware

Sub-system input/output includes information passing through the analog and digital boards. This task handles the sub-system control and/or monitoring not handled through the Ethernet link. An example is the control of various applicator peripherals. The sealant temperature would be controlled by the user through an analog channel. The user specified temperature is translated to the pre-determined analog channel, which directly connects to the sealant temperature controller. These I/O tasks are handled by some routines within the icudata.c module accessing the XVME201 (Digital I/O) and XVME540 (Analog I/O) cards.

Set-up: A hardware testbox was built to simulate various input and output devices. Software modules were developed on the ICU to control the analog and digital I/O cards. Connection between the test box and the ICU was through ribbon cable. Figure 2.2 shows the setup described above.

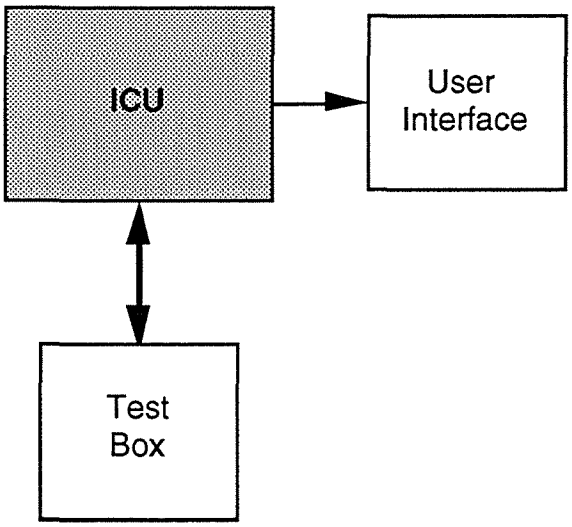

Figure 2.2 *- Experimental Set-up for ICU Test 3.*

Procedure: The ICU obtains status information from the test box and sends control information to it. Switches and rotary potentiometers on the box change screen (user interface) counterparts. Control information from the ICU is communicated to the box resulting in test box indicator status changing. Several simultaneous inputs and outputs are accommodated.

2.2.4 - Test 4: Machine Control from the Real-Time User Interface

The user interface allows control of the machine and displays the status of the ACSM in real-time. Interactive slidebars and buttons on the user interface provide controls such as switching the heater on and off and setting and changing temperature and level parameters on the heater and dispenser. With the use of graphical meters and buttons, the user screen also displays status and emergency indicators. The icudemo.c module, developed in part by the RAVE software, uses the MMI250 (Audio/Graphics) card to affect a friendly user screen.

Set-up: An interactive user interface was developed using realtime audio-visual software along with a graphics card. This software interacts with the I/O software to display control information from the test box. It also passes user input to the I/O cards.

Procedure: User input, from a mouse, is used to change status of the box hardware by clicking and dragging various indicators on the user interface. Knobs and switches on the test box are used to change the status of various indicators on the screen. All controls and indicators can be used and are updated simultaneously. The user interface displays the VSS data in a window as and when the data is received from the VSS.

2.2.5 - Test 5: Environmental Testing of the Hardware

The ICU hardware should withstand the vibrations, shocks, and temperatures typically present in a heavy truck environment. We had intended to test the ICU hardware to the specifications provided by the manufacturers and recommend appropriate ruggedization measures based on the results. This environmental testing and ruggedization has been postponed to a time when the loss of any equipment use is not so detrimental to the completion of the project. Therefore, the environmental testing has been rescheduled for Phase III.

2.3 - Results

2.3.1 - Test 1: Acceptance Testing of the Delivered Hardware

Acceptance testing of all component boards has been completed. The system backplane (HSE/17R) appears to function as specified. Approximately one-third of the backplane is currently occupied by the ICU hardware, allowing the flexibility to house other subsystem processors as well as the VSS hardware at some later date. The analog I/O card (XVME540), the digital I/O card (XVME201) and the communications card (CMC ENP-10) performed as expected during all acceptance tests. Two

problems were uncovered during testing of the CPU card (HK68H/V3E). The first problem was a lack of on-board Random Access Memory (RAM) to allow complete functional operation of the operators' user interface. The second problem was an occasional unexpected system error causing the complete system to lock up. This problem was traced to the CPU, and the board has been sent back to the manufacturer for warranty replacement. At the same time, the manufacturer will upgrade the RAM to allow full functionality of the user interface. The team has also uncovered a problem with the user interface multi-media graphics card (MM1250). The team is working with the manufacturer to solve this problem and is not expected to impact project progress.

2.3.2 - Test 2: Data Communications with Other ACSM Subsystems

Communications between the simulated VSS and the ICU via the Ethernet has worked as expected . Real crack information was passed in a simulated manner to the ICU and displayed on the user interface. Although this task was simulated, it reflects in every manner the actions that will take place when passing information from the VSS to the ICU and from the ICU to the RPS and User-interface. Total integration of the VSS and ICU will be complete with the installation of a communication card on the VSS backplane.

2.3.3 - Test 3: Input/Output Interfacing with Test Hardware

Control information from the ICU was used successfully to change status of indicators on the test box. Sensor information from the box was used successfully to change status of indicators on the screen. This test positively simulated the transfer of information from any other subsystems to the ICU. This information was not only sent at varying rates, but multiple information was also sent thus testing the multi-tasking functionality of the CPU.

2.3.4 - Test 4: Machine Control from the Real-Time User Interface

User input and control information from the user interface was used successfully to change information on the hardware test box. Both auditory and visual information was given to update the user on the status of various indicators and alarms. This test performed as expected.

2.3.5 - Test 5: Environmental Testing of the Hardware

As described earlier, the environmental testing will be conducted during Phase III of the project. The team does not anticipate any failures based on information obtained from past users of this equipment type. In the event of a failure, the team now has at its disposal duplicate hardware.

3.0 - VISION SENSING SYSTEM (VSS)

3.1 - Objective

The purpose of the Vision Sensing System (VSS) is to locate pavement crack positions using machine vision. This section concisely describes testing of the VSS during Phase II of the project. This included both laboratory and on-road testing through the use of the Odetics Corporation's Mobile Imaging (Sensor) Laboratory. This laboratory is a truck with enclosed bed that contains adequate power, air conditioning, monitors, tape recorders, and other electronic equipment and mountings for vision system testing, and in particular, it contains Datacube vision processing equipment and support computers totally compatible with our vision system hardware. The functional aspects of the VSS, including physical description of the system, its components, and a description of how it relates to other parts of the automated crack sealing machine (ACSM) have been discussed previously.

The VSS consists of two cameras, lighting, an encoder, and system unit which encompasses image processing hardware and crack detection algorithms. The VSS is to identify cracks greater than .20 inch wide on PCC (Portland Cement Concrete) and AC (Asphalt Concrete) roadways. The intent of the crack recognition testing is to examine the accuracy of the VSS in identifying crack location and direction in the two kinds of pavements.

The first issue to examine is lighting. The efficiency of crack detection is dependent on controlled lighting. Orientation of lamps, dispersion and adequacy of lighting, affect the display of cracks in contrast with the pavement, which is significant for the cameras to extract a flawless image for crack recognition processing.

The next issue is the dependability of the encoder. As the wheel of the vehicle incrementally rotates up to speeds of 2 miles per hour, an encoder, attached to the hub, produces a pulse every .0625 inches of travel. The encoder must filter out noise and accurately track the distance regardless of speed.

The last issue is the evaluation of video acquisition and CPU processing time constraints. Real-time processing is essential to coordinate accurate crack location and direction. Image processing hardware takes the pulse and sends control signals to two cameras (combined to scan a 12 foot wide lane) to acquire a line of video data. A video signal representing one line of pavement is sent back to the image processing hardware. After a sufficient number of lines have been gathered, the crack detection

algorithm will use this set of information to group pixel gray-scale data into two inch square sections of tiles. The data contained in each tile is transformed into a histogram. A statistical moment calculation then converts the data into a single number representative of the contrast present in the tile. Comparisons with the 24 nearest tiles leads to the determination of the presence of a crack in addition to its general direction. If a crack is detected, its location and direction is transmitted via Ethernet to the ICU (Integration and Control Unit) for path planning and verification by the Local Sensing System (LSS).

3.2 - Requirements

VSS performance is judged by the criteria presented in Table 3.1.

3.2.1 - Lighting

Through a contract to Odetics Corporation, requirements for lighting were determined and a lighting structure was built to optimize intensity and orientation of the lights necessary for proper illumination of the roadway surface to achieve high resolution images. In order to read both transverse and longitudinal cracks, the light falling on the surface should be non-directional. The only true source of non-directional light is sunlight. The goal of the study was to determine which commercially available lighting system would best simulate this non-directional lighting.

Table 3.2 shows the comparison of performance for the three most viable white light sources. The fluorescent light is useful in creating a bright light source, but will have to be used in conjunction with a high frequency ballast in order to compensate for the discontinuous light emission (strobe light effect). The performance output level is 2800 lumens per 40 watts, without the ballast. The high pressure sodium lamp has broad spectral content from 550 to 700 nanometers, with the majority of the light (close to 75 percent) being between 580 and 630 nanometers which is a good range for solid state video cameras. These lamps require a start up time of a few minutes and a ballast. The high frequency ballast for both the fluorescent and high pressure sodium lights can add $200 to $500 to the cost of a single unit. For our test purposes, Halogen lamps will prove to be the more feasible and more cost effective choice.

A program was written to predict illumination reflected from the pavement and measured at a single camera for different lamp configurations. Based on photometric measurements from a single pair of lamps, the program calculates the light distribution in foot-candles.

RESOLUTION ALONG SCAN/ENCODER PULSE	1/16"
VERTICAL RESOLUTION	1/16"
FIELD OF VIEW	12' 8"
CAMERA DISTANCE TO SURFACE	6'
CAMERAS MUST ENDURE	15 G from 5 Hz to 60 Hz vibration 150 dB noise environment 10% humidity sand & dust salt atmosphere sea level to 10,000 ft. altitude .7 ms exposure time
IMAGE PROCESSING MUST DISTINGUISH	cracks oil spots shadows
CRACK RECOGNITION	.2" to .6" wide >10" length 70% recognition
CONTINUOUS MOVEMENT OF VEHICLE	0-2 mph
CONTROLLED LIGHTING	50% to 75% saturation min. 4500 foot-candles intensity 28" from surface operate and tolerate: direct sunlight rain and freezing conditions
SYSTEM RESPONSE FREQUENCY	18 Hz
SERVICE LIFE	10 yrs

Table 3.1 - *Vision Sensing System Requirements.*

The noted simulation was exercised to examine a variety of lighting configurations. Illumination was considered for various numbers of lamps and the heights of those lamps from the pavement. The curves shown in Fig. 3.1 provide an indication of the variation in illumination as a function of lamp height. Specifically, we are concerned with illumination intensity and uniformity. This simulation considers the full lane width

field of view (156 in.) as seen by a single camera located at the center of the left half of that field of view. In the actual VSS, there are two cameras, one in each half of the field of view, and thus we are only concerned with the useable illumination for that camera - the left half 78 in. Based on symmetry of the VSS, the illumination for the right camera will be the mirror image of the left half 78 in. In general, for a fixed number of lamps, the illumination level will be higher the closer the lamps are placed relative to the pavement. However, there will be a corresponding loss of uniformity in the lighting. Based on the use of this simulation, 7 lamp pairs located at a height of 28 inches from the pavement was selected as the first generation lighting configuration for the VSS testing of Phase II.

3.2.2 - Cameras

The cameras must have sufficient resolution to consistently recognize cracks .2 in. wide. The field of view transverse to the vehicle is covered by two cameras (Fairchild CAM 1301R CCD Line scan cameras with JML P/N 71846 12.5 mm, f1.3 lenses) mounted 6 feet from the ground. Each camera has a field of view of 6.4 ft. and they are mounted 6.4 ft. apart. Each camera's field is divided into 1024 elements representing .075 in., for a Nyquist resolution of .15 in.

3.2.3 - Encoder

The encoder must trigger a line of video every .0625 in. The video acquisition is driven by the forward travel of the vehicle using a 1000 pulse per revolution optical encoder from Datron Technology. The rolling radius of the wheel on which the encoder is attached is 13.25 in. resulting in a pulse every .0835 in. and pixel spacing of .0835 in., in the forward traveling direction of the vehicle. Therefore, the theoretical Nyquist resolution of the image is .167 in. which is 20% better than the .20 in. crack width required of the system.

SOURCE	OUTPUT	OUTPUT VIS/ALL (*power/cm^2*)	LIFETIME	COMMENTS
fluorescent	2800 lumens/40W	10mW/12mW @2"	12000 hrs	extended, uniform sources
halogen	5000 lumens/300W	.45mW/1mW @10'	1500 hrs	hot lamp
high pressure sodium, clear bulb	15000 lumens/150W	140mW/155mW @4"	24000 hrs	bright light source

Table 3.2 - *Comparison of Performance for Various White Light Sources.*

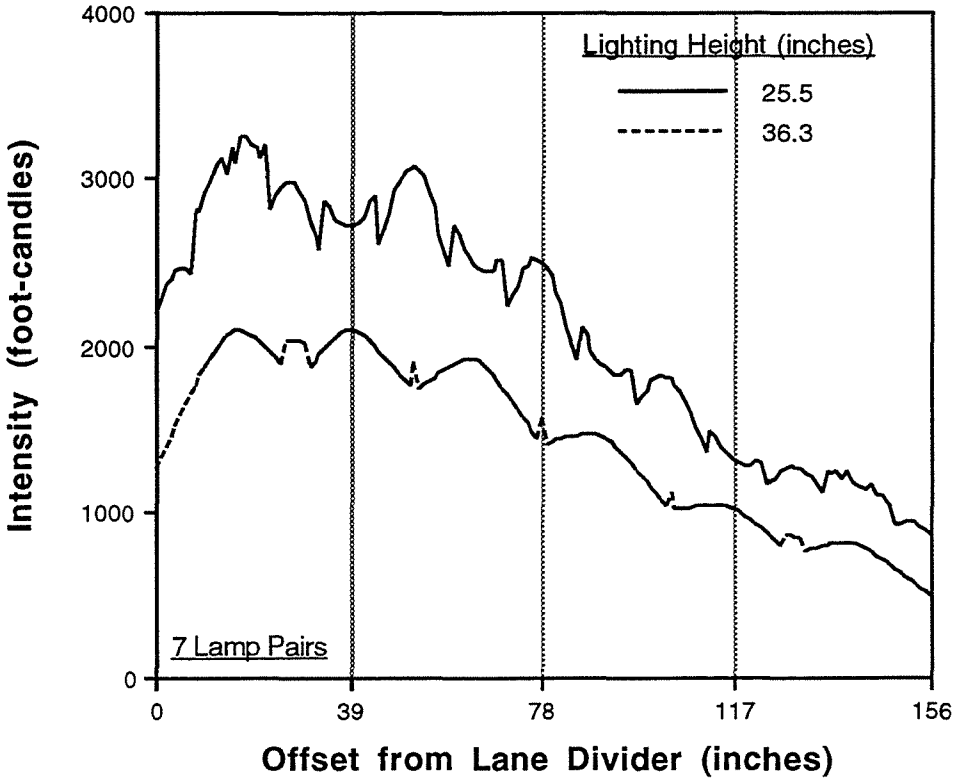

Figure 3.1 - *Examples of Simulated Illuminations for VSS Lighting.*

3.2.4 - Image Processing Hardware and Software

In order to produce accurate data for external (outside VSS) processing, the image processing hardware and software must interact efficiently. The encoder and cameras supply accurate data to the image processing boards. Upon a rising edge pulse of the encoder, a line of video from each camera is sent to the MaxScan card. Next, raw data is sent to the ROI 512 and ROI 2048 cards. The ROI 512 processes the data which is transferred to MaxGraph for visual observation. The ROI 2048 utilizes the same data to process pertinent information into FeatureMax MKII for crack identification.

The information for crack identification is implemented into an algorithm which will interpret the presence of a crack by statistical means. The presence of a crack is determined by establishing its width and length. Cracks less than .2 in. wide and less than 10 in. in length are rejected. Acceptable crack information along with its location and direction are transferred for external processing. Seventy percent of the cracks

are expected to be recognized and deemed acceptable. Prior static testing indicates that this algorithm is functioning as expected.

3.3 - Method

3.3.1 - Set-up

The on-road testing was conducted with the use of the Odetics Corporation's Mobile Imaging Laboratory (MIL). The MIL consists of a truck with enclosed bed that contains adequate power, air conditioning, monitors, tape recorders, and other electronic equipment and mountings for vision system testing. In particular, it contains Datacube vision processing equipment and support computers totally compatible with the vision system hardware purchased for the crack sealing project.

The use of the MIL during the testing phase of this program will closely replicate the conditions and situations that will be present during operation of the actual crack sealing machine. This includes the identification of actual pavement cracks on secondary roads in and around the greater Los Angeles and Sacramento areas. Following tests, all equipment including lighting, encoder, cameras and image processing hardware and software will be directly transferable to the actual crack sealing machine with minimal modifications.

The Odetics Corporation MIL will contain the following equipment:

- A frame support and frame structure for a lighting system and cameras which will occupy a maximum space of 8 ft. x 8 ft. x 3 ft. and weigh approximately 400 lbs. The mounted configuration of the lighting, frame, and cameras will conform to current vehicle codes. Mounting of the frame, lighting system, and cameras will be performed by Odetics.
- Electrical power for computer and camera equipment (1500 W, 110 VAC, 60 Hz).
- Mounting within the vehicle: a 19 in. x 19 in. rack mountable VME computer weighing approximately 80 lbs., two 14 in. monitors, an extended keyboard, and routing of several cables to the exterior of the vehicle.
- Environmental control within the vehicle to keep storage temperatures within -40° to 85°C and operating temperatures within 0° to 55°C
- A TTL pulse transducer to the VME computer corresponding to an incremental vehicle travel of approximately 1/16 in.

Figure 3.2 shows the rear of the Odetics MIL with the first generation VSS lighting and cameras mounted.

3.3.2 - Flow Diagram

Figure 3.3 pictorially describes the functional aspects of each component in the Vision Sensing System. The corresponding sequence of events taking place in the VSS is as follows:

1. Wheel rotates an incremental amount.
2. Encoder produces a pulse resulting from incremental vehicle travel.
3. Image processing hardware reads pulse from encoder.
4. Control signal sent to notify camera to acquire video line.
5. Camera returns a video signal representing one line of pavement back to the image processing hardware
6. Procedure (1. - 5.) repeated until enough lines are gathered to determine implement crack finding algorithm.
7. Crack finding algorithm implemented and determines crack presence in image (in local areas called tiles) and transmits crack information to the ICU.
8. Crack information is communicated to path planning function (external to VSS).

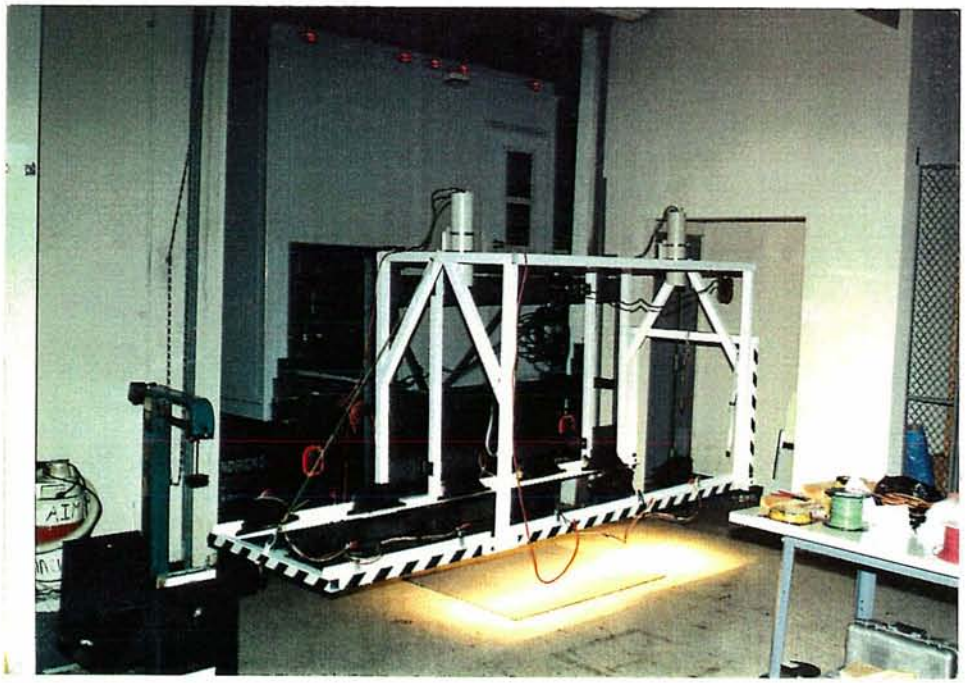

Figure 3.2 *- Odetics MIL with Cameras and Lighting.*

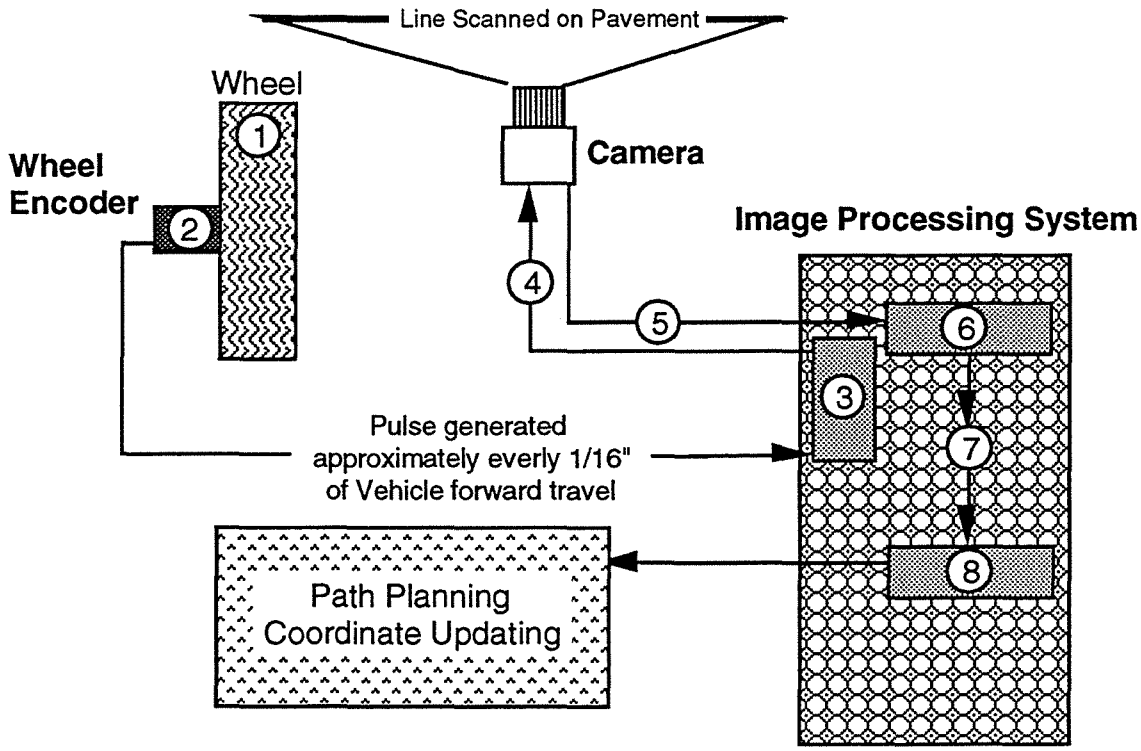

Figure 3.3 *- Vision Sensing System Flow Diagram.*

3.3.3 - Test Procedure

The MIL, outfitted with all the appropriate vision sensing hardware and software will attempt to recognize cracks that are .2 in. or greater while the MIL is in forward motion. Vehicle speed is not to exceed 2 mph. Following is a more detailed test plan:

1. A secondary road will be selected in which to perform crack identification. The road must possess a series of both longitudinal as well as transverse cracks relative to vehicle travel. The cracks must exceed .2 in. width and 10 in. length. All cracks will be physically measured prior to system identification including a random assessment of width to identify cracks that are primarily .2 in. or larger. These cracks will be identified by placing a marker on the road just prior to the crack. This information will be used for laboratory data reduction. Note that the VSS not only provides crack location and direction, but constructs an actual video image of the road surface. The road marker is present in these images and will be recorded on a videocassette tape.

2. Initially, the MIL will travel in the forward direction in increments of 10 in. and identified crack locations will be compared to physically measured crack locations. Approximately 30 to 50 cracks will be assessed.
3. Procedure one will be repeated until results are satisfactory which occurs when nearly all of the individual crack is recognized and it is apparent that a path planning function can eliminate the noise and fill in the gaps of recognized crack locations. A goal of 70% recognition along the length of an identified crack has been assigned in addition to a maximum 20% noise level. The use of 70% recognition along the length of an identified crack as a target is reasonable in light of the roles of the path planning algorithm and the local sensing system which will provide the remaining information allowing the entire crack to be addressed.
4. The MIL will then travel continuously through the series of pavement cracks. The maximum speed will be documented along with any associated crack identification problems.

3.4 - Results

Following the development and static checkout of the MIL with all associated vision equipment at Odetics Corporation in Anaheim, CA., dynamic testing was to occur in the greater Los Angeles area. This was to be an initial debugging session prior to a demonstration to SHRP participants in Sacramento. Because of inclement weather, testing was delayed in Los Angeles and the MIL was shipped to Sacramento one day prior to the scheduled demonstration. For these reasons, actual testing was completed after the Sacramento demonstration on a secondary road near downtown Sacramento. It is worth noting that identification of a section of secondary road with transverse as well as longitudinal cracks of width greater than .2 inches was a difficult task in and around Sacramento. Caltrans maintenance crews as far north as Lake Tahoe, and as far south as Stockton were queried to identify sections of road that fit test specifications. The general response was that cracks of this size were already sealed, or reside on primary roads such as freeway lanes. Testing on primary roads has been reserved for final machine testing in order to minimize traffic congestion and costs resulting from extended lane closures.

Accordingly, testing was conducted on a two lane road along a levy west of Sacramento. This section of road had minimal vehicle travel, but had a series of transverse and longitudinal cracks meeting test specifications. In order to minimize the effects of ambient lighting, the initial testing for crack identification was conducted at

night. This was to be followed by daytime testing if all test results proved acceptable. If a significant disparity between the nighttime and daytime testing resulted, the camera and lighting system would be shrouded prior to further daytime operation. The outriggers on the lighting bar for extending the light to the full 13 foot lane width were not used because of the limited lane width. This limited identification to a maximum of 8 feet with possible unknown fringe effects due to inconsistent lighting at the edges. This information could be filtered by limiting the region of interest (ROI) when reducing the data for analysis.

At least 40% of the cracks in this series were evaluated as acceptable prior to being scanned by the vision system. A crack was considered acceptable if it was at least .2 in. wide for most of its length. A simple gage of .2 in. width was inserted into the crack at numerous locations along its length to determine acceptability. Acceptable cracks were identified by placing a piece of white tape on the pavement next to the crack. A video recorder was connected to the monitor to record the video image of the cracks along with the crack recognition indicators.

3.4.1 - Lighting

The lighting configuration was directed forward and to the rear of the vehicle. This was an initial configuration to determine if longitudinal cracking would be "washed out". During the testing, one test site was found with longitudinal cracking and the performance was poor. Lighting that is more indirect along with the deivision of the camera fields of view may improve performance on longitudinal cracking; however, longitudinal cracking at the extreme edges of a lane may remain difficult to detect.

3.4.2 - Encoder

The encoder performs exceptionally well at speeds up to two miles per hour. At operational speeds the encoder provides for a clear image. At slow speeds the video lines tended to darken and sporadic movement of the vehicle at very slow speeds produces dark bands which are occasionally identified as transverse cracks. Additionally, a circuit was previously constructed to reduce encoder noise. During testing it became apparent that this circuit also has the effect of sporadically incrementing video as the vehicle moves backwards. This typically occurs when the vehicle idles causing the encoder to oscillate backwards and forwards.

This is not a significant problem as many applications exist using line scan video technology linked to motion encoders. It appears that more significant filtering at slower speeds might eliminate the sporadic dark lines. Additionally, a filter will be constructed to limit line scanning to forward vehicle motion only.

3.4.3 - Cameras

During accelerations and decelerations of the MIL, the video image became lighter and darker, respectively. This was reflected on video as dark bands and recognized as transverse cracks. The cause is likely encoder noise which corrupts the leading edge of the triggering pulse. Worth noting was that a difference in video level between the two cameras appeared as a longitudinal dark band which was not identified as a crack indicating system robustness.

3.4.4 - Hardware and Software Image Processing

The resolution of the system on transverse cracks was required to be .2 inches. The calculated value for transverse resolution was approximately .0625 in. due to the radius of the wheel upon which the encoder was attached. Every transverse crack that was sufficiently wide was mostly detected. These cracks were not recognized well at the outer edges of the fields of view. One reason is that the tests that were performed did not make use of the lighting outriggers which would have provided additional lighting and hence additional contrast at these edges. Figure 3.4 is a schematic showing typical system performance for a transverse crack. Figure 3.5 shows examples of actual processed images. Both are well recognized transverse cracks. Ther images show the dark bands along the outer edges of the field of view indicative of the lack of extension of the lighting outriggers. Relative lighting unifomity is apparent in the remainder of these images.

The best way to describe the image processing performance is to consider the individual performance of the two comprising groups, the Algorithm/CPU group and the CPU/Image Processing group. Currently, the overall system is able to perform at vehicle speeds as high as 1 mph. Sixteen percent of the vision system operation is consumed by the Algorithm/CPU group. During this time computations are made based on the data retrieved through the CPU/Image Processing Group. The

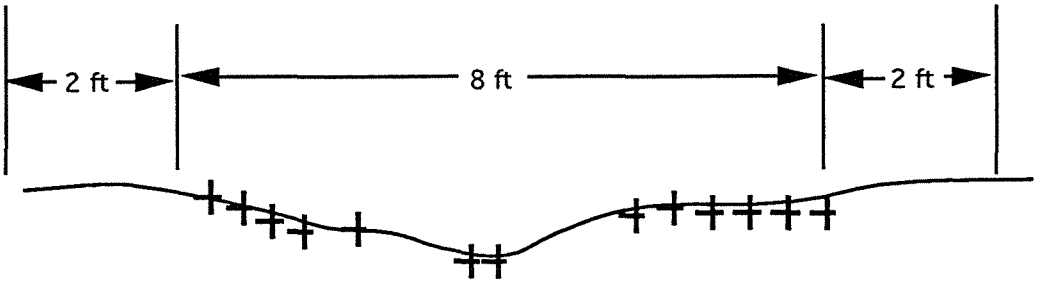

Figure 3.4 - *Typical VSS Performance for a Transverse Crack.*

remaining 84 percent of the operation time is spent by the CPU/Image Processing group. During this time registers on the image processing boards are written to and read by the CPU. Two critical functions of the CPU/Image Processing group are reading and writing to registers containing the histograms (56 percent).

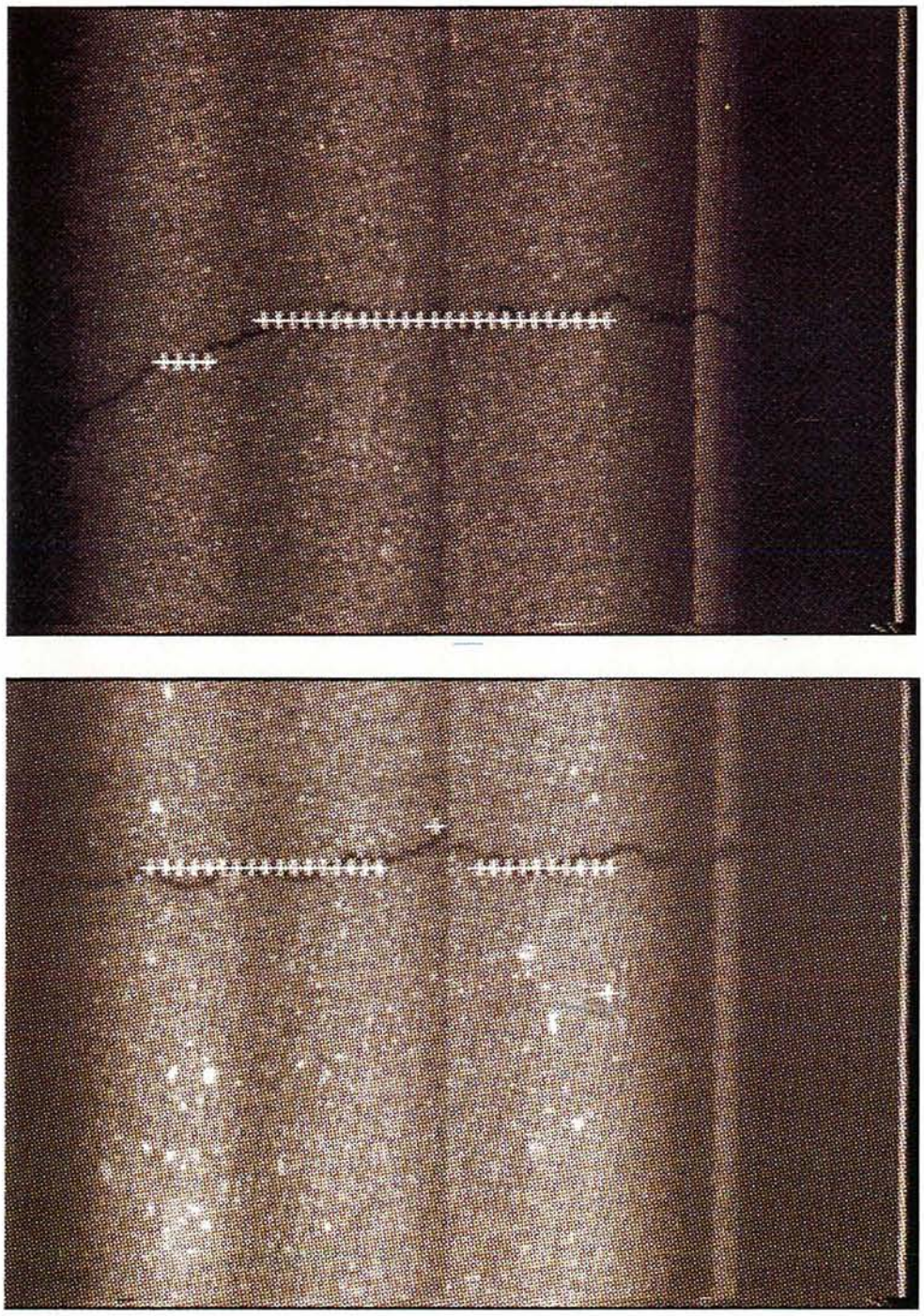

Figure 3.5 - *Processed Crack Images.*

3.5 - Conclusions

The data acquired during the testing portion of this phase indicates moderate overall performance. Data for 32 cracks was acquired through testing with the Odetics MIL. Of these 32 cracks, 19 were primarily wider then .2 in. The remaining cracks were primarily less then .2 inches. The chart in Fig. 3.6 indicates that the system identified, on average, 64% along the length of each recognized crack that was at minimum .2 in. wide. As noted earlier, the target identification percentage was set at 70% under the assumption that the remaining 30% would be addressed through the path planning algorithm in conjunction with the LSS. Additionally, the system was only tested at night as the results in this optimum configuration (no ambient light) were less than targeted. The top speed of the MIL to achieve adequate results was 1 mile per hour. The insufficiency of the VSS arises from several aspects which along with our approach to their solution during Phase III are now discussed.

The lighting structure assembly appeared to provide adequate lighting for the line scan cameras. As shown in the recorded images, some lighting overlap exists as indicated by a contrast change in the image. This does not appear to be affecting the cameras or detection algorithm, but further testing with different light heights, angles, etc. should help to eliminate this effect. Furthermore, the camera's image appeared to be distorted at its edges which is attributable to the fact that the lighting boom extensions could not be used due to the lane width limitations. Further testing with the booms extended will be performed to examine this aspect. As the system was only tested at night, the need for a shrouded structure has not yet been ascertained.

The encoders were not designed to incorporate 1/16 inch resolution. Higher resolution encoders will be used in future testing. Additional filtering of noise should eliminate sporadic lines erroneously detected as cracks.

Changing speeds caused dark bands in the video image due to changes in the triggering rate of the cameras. This led to false positive crack recognition. Further encoder filtering will be pursued to eliminate this problem.

Several hardware/software improvements could be implemented in Phase III to improve the speed and accuracy of the identification process. A new upgraded CPU could be purchased that would reduce the Algorithm/CPU processing time by 75%. In addition, image processing hardware source code will be revised to reduce the register access time by 50%. With both of these improvements, the VSS will work effectively at speeds up to a maximum of 2.17 mph. With just the image processing source code modifications, the VSS will work effectively at speeds up to a maximum of 1.47 mph.

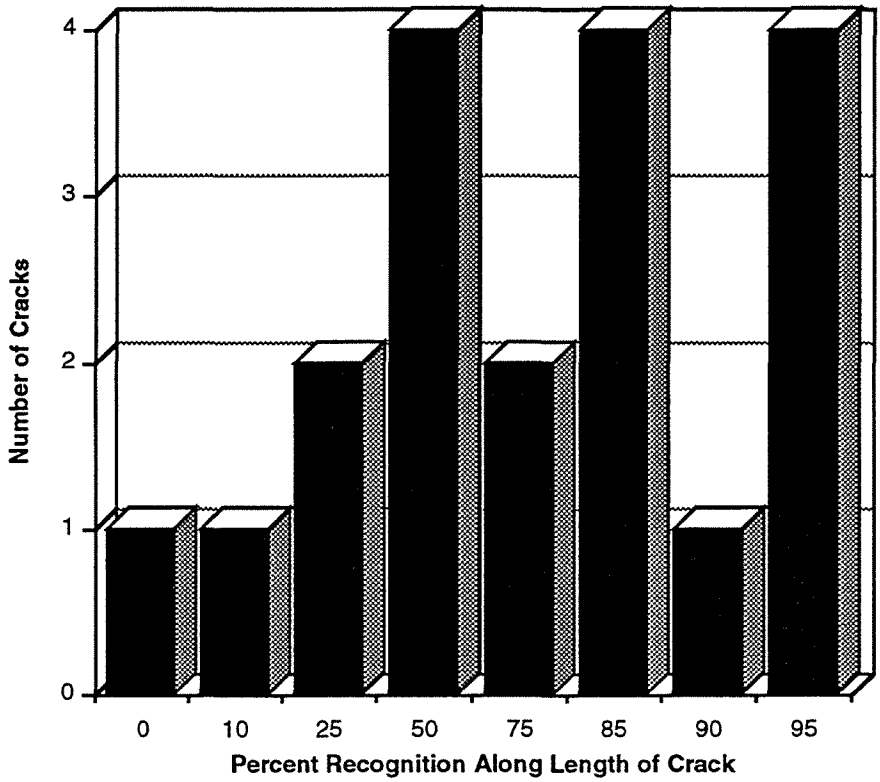

Figure 3.6 - *System Crack Detection Performance.*

3.6 - Further Testing

The testing that was performed was adequate to identify the working level of the vision subsystem, indicate several aspects that limited system performance, and provide an indication of probable solutions to attain desired performance. Due to the necessity for continued VSS testing and the logistics associated with the additional use of the Odetics MIL (i.e., location, time and cost), Caltrans has agreed to build its own Mobile Imaging Laboratory that will be available to the crack sealing project at no cost. The completion of the Caltrans MIL is expected during August, 1992, and this date will fit the schedule for VSS hardware/software modifications. The MIL will be outfitted with all of the associated equipment used on the Odetics MIL including a larger generator and adjustable lighting and camera mountings. This design will allow additional operator flexibility in adjusting peripheral components. It is anticipated that component optimization will progress rapidly during the final modification/testing phase due to this facility.

4.0 - LOCAL SENSING SYSTEM (LSS)

4.1 - Objective

The objective of the experimental verification is to test the instrument response of the LSS. The instrument response is considered to be output produced for a given input. The input into the system is the absolute location of a crack in the surface being measured. The output of the system is the crack location generated by the LSS hardware and software. Additionally, the LSS must output a signal when no crack is located in the surface being measured, or the crack in the surface is either too small (<1/8") or too large (>1-1/2") to seal. The LSS must produce viable output for all expected input under a variety of different operating conditions. This output must meet the requirements shown in Table 4.1. Before output characteristics of an instrument can be analyzed, the instrument must be calibrated. Calibration procedure consists of determining output for a given input over the range of inputs which the instrument is to be used. This will be accomplished by comparing the response of the LSS to known input. A problem arises in that the known input is considered to be the true input, while in reality it is affected by the response of the measuring instrument which is determining the input. Therefore, to produce a meaningful calibration results, the instrument used to measure the input must have better response than the system being calibrated.

From the calibration data, a calibration curve, or a plot of the instrument output versus the input over the usable range, will be generated. A best fit line will be generated through the linear region of the plot using least squares method. From this curve, the sensitivity, linearity, bias, and accuracy of the LSS will be determined. Sensitivity (also referred to as gain) is the slope of the calibration curve in the linear region. Linearity is the departure of the calibration curve from a straight line relationship. Bias, or systematic error, is a common offset to all readings, corresponding to the y intercept of the calibration curve. Finally, accuracy is the ability of the instrument to produce an output which corresponds to the true input. To quantitatively measure the accuracy, a percent error will be calculated. The percent error is defined as the difference between a given data point and the calibration curve. The value will be expressed as a percent of the instruments full scale reading, using the point which strays most from the calibration curve.

Once the calibration curve has been generated, the precision, or repeatability, of the Local Sensing System will be determined. Precision is defined as the ability of an instrument to produce consistent output for a given input. This will be accomplished by measuring crack location using the LSS. Enough points will be measured so that a normal curve can be generated. From the data, the sampled standard deviation of the sample will be calculated. The sampled standard deviation is defined by:

$$s = \sqrt{\frac{\sum_{i=1}^{N}(X_i - \overline{X})^2}{N - 1}} \tag{4.1}$$

where

$$\overline{X} = \frac{\sum_{i=1}^{N} X_i}{N} \tag{4.2}$$

and

X_i = individual reading,
N = total number of readings,
s = sample standard deviation, and
$\overline{X}$ = sample mean average.

For a perfect Gaussian distribution, the following relationship arises:

68% of the readings lie within +/-1 standard deviation of the average,
95% of the readings lie within +/-2 standard deviations of the average, and
99.7% of the readings lie within +/-3 standard deviations of the average.

Typically, a 95% confidence level is used as a measure of the precision of the instrument.

Once the static instrument response has been determined, a variety of tests will be performed. The objective of these tests is to ensure proper performance of the Local Sensing System under different operating conditions. Specifically, the sensor must have the ability to distinguish between oil spots, shadows, previously sealed cracks, and actual cracks under different lighting conditions. The sensor must produce reliable and accurate results which meet the requirements shown in Table 4.1.

4.2 - Requirements

Sensor performance will be judged by the following criteria. The output of the sensor must meet the specifications in Table 4.1 under all test conditions.

RESOLUTION ALONG SCAN	1/16" (1.588 mm)
VERTICAL RESOLUTION	1/16" (1.588 mm)
FIELD OF VIEW	4" (101.6 mm)
DISTANCE TO SURFACE	4" (101.6 mm) minimum
SYSTEM RESPONSE FREQUENCY	18 Hz
HUMIDITY	to 85%
VIBRATION	3 G peak from 15 Hz to 100 Hz
SHOCK	10 G
OPERATING TEMPERATURE	32 to 160° F (0.0 to 71.1° C)
SERVICE LIFE	10 yrs
SENSOR MUST ENDURE	• wind and sunlight • dusty environment • surface color variations • moisture on pavement • debris in cracks • road surface height variations • temperature variations • electromagnetic interference
SENSOR MUST DISTINGUISH BETWEEN	• previously filled cracks • oil spots • shadows • actual cracks

Table 4.1 - *Sensor Requirements.*

4.3 - Method

4.3.1 - Set-up

In order to perform the experimental verification, the hardware and software shown in Table 4.2 are necessary.

In order to perform the static calibration procedure, the sensor will be mounted on a robot arm. Using a teach pendant and the robot controller, it is possible to very accurately position the sensor. The surface being measured will be a piece of plywood board containing a 7/8" routed crack. The precision measurement procedure will also be performed while the sensor is mounted on the robot arm. Again, the

surface being measured will be the same piece of plywood. A photograph of the sensor mounted on the robot arm is shown in Figure 4.1.

To accomplish the performance tests, the sensor will be mounted on a test apparatus. The test apparatus allows the sensor to be placed at any desired position over the surface being measured. Furthermore, the sensor will be mounted 3-3/4" from the surface being measured. A photograph of the test apparatus for the performance tests is shown in Figure 4.2.

One Laser Vision Sensor
One 30mW laser source
One sensor and laser power supply
One Laser Vision Image Processor
One co-processor board
Crack identification program
PCC sample containing a crack between 1/8" to 1" wide
AC sample containing a crack between 1/8" to 1" wide
PCC sample containing a sealed crack
AC sample containing a sealed crack
Robot, robot controller, and teach pendant
Laser Vision Sensor mounting bracket
Plywood board containing a 7/8" route
IBM compatible 386-25 MHz
Test apparatus

Table 4.2 - *Hardware Requirements for Experimental Verification.*

4.3.2 - Interconnect Schematic

The system connections are shown in Figure 4.3. The power supply requires an external 110 VAC source, which will be provided by a standard outlet. A cable will run between the power supply and the laser vision sensor, which will provide power to the camera and laser, and will provide a synchronization pulse to the camera.

The image processing board and co-processor will both plug into a standard slot in the IBM compatible computer. There is a cable connection between the image processing board and the co-processor. A second cable runs from the sensor into the computer to the image processing board. The data collected by the sensor enters the

computer via this cable. The computer also requires an external 110 VAC power source.

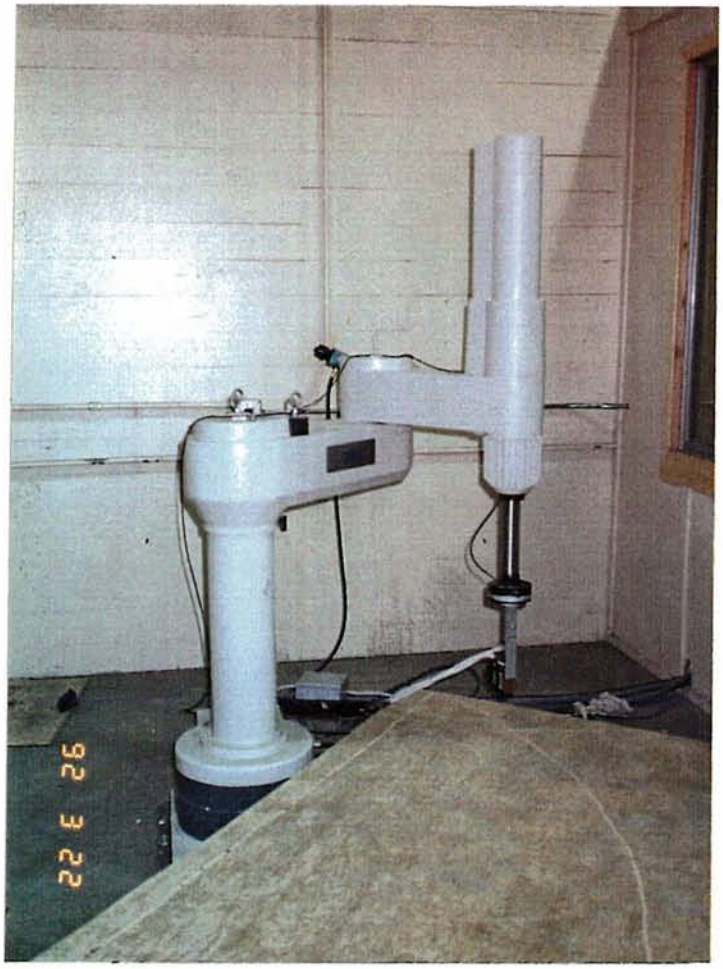

Figure 4.1 *- Sensor Mounted on Robot Arm.*

4.3.3 - Test Procedure

The following procedure will be performed to confirm sensor performance. First, static instrument response of the Local Sensing System will be determined. Data will be collected to produce a calibration curve and thereby determine the LSS sensitivity, linearity, bias, and accuracy. Next, the precision of the LSS will be determined by measuring the many output points for the same input. Statistics will be performed on the data to determine the sample standard deviation and the precision of the instrument. Finally, the performance of the local sensor will be determined in a variety of operation conditions. The procedure will be performed over four pavement samples under two different lighting conditions, corresponding to eight experimental runs. The

four pavement samples include a PCC pavement section containing a crack, an AC pavement section containing a crack, a PCC pavement section containing a sealed crack, and an AC pavement section containing a sealed crack. The experiment will be run when the pavement sample is exposed to direct sunlight and when the pavement sample is located in the shade. Profile data and crack location will be collected and stored for analysis. Each test run will last 300 seconds.

Figure 4.2 - *Performance Test Apparatus.*

4.3.3.1 - Static Calibration Procedure

1. Connect the hardware as shown in Figure 4.3.
2. Mount the sensor on the robot arm as shown in Figure 4.1.
3. Place the sensor over the center of the routed crack so that the direction of laser light is perpendicular to the direction of the routed crack.
4. Using the teach pendant, adjust the height of the sensor so that the bottom edge of the sensor is 3-3/4" above the surface being measured.
5. Record a measurement corresponding to crack location.
6. Move the sensor 2 mm perpendicular to the crack direction using the teach pendant.
7. Record another measurement corresponding to crack location.

8. Continue taking measurements every 2 mm until the crack is no longer in the field of view of the sensor.
9. Return sensor to the start point over the center of the crack.
10. Record a measurement corresponding to crack position.
11. Move the sensor 2 mm in the opposite direction as previously performed in step 5.
12. Record another measurement corresponding to crack location.
13. Continue taking measurements every 2 mm until the crack is no longer in the field of view of the sensor.
14. Repeat procedure for a second set of calibration points
15. Perform least squares curve fit on linear portion of data to produce curve fit.
16. Plot data points and calibration curve.
17. Determine sensitivity, linearity, bias, and accuracy.

4.3.3.2 - Precision Measurement Procedure

Next, the precision of the LSS will be determined. To determine the precision of the LSS, the following steps will be performed.

1. Connect the hardware as shown in Figure 4.3.
2. Mount the sensor on the robot arm as shown in Figure 4.1.
3. Place the sensor approximately over the center of the routed crack so that the direction of laser light is perpendicular to the direction of the routed crack.
4. Using the teach pendant, adjust the height of the sensor so that the bottom edge of the sensor is 3-3/4" above the surface being measured.
5. Record 300 measurements of crack location at this location.
6. Move the sensor over approximately 10 mm perpendicular to the direction of the crack using the teach pendant.
7. Record 300 measurements of crack location at this location.
8. Move the sensor 20 mm in the opposite direction, so that the sensor is -10 mm from the center of the crack.
9. Record 300 measurements of crack location at this location.
10. Determine sampled standard deviation for the three sets of sampled data.

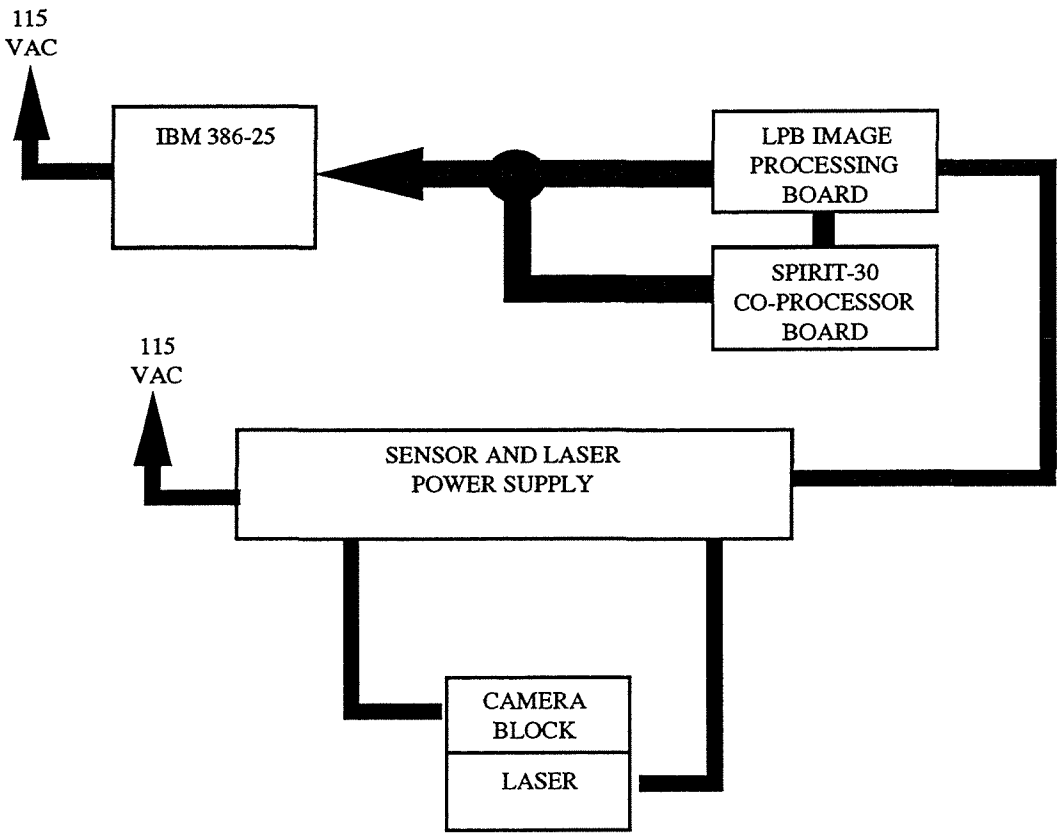

Figure 4.3 - *Local Sensing System Device Connections.*

4.3.3.3 - Performance Testing Procedure

Finally, the performance of the LSS under different operating conditions will be determined. To measure sensor performance, the following procedure will be performed on both AC and PCC pavement samples:

1. Connect hardware as shown in Figure 4.3.
2. Mount the sensor on the test apparatus 3-3/4" from the surface being measured as shown in Figure 4.2.
3. Place test apparatus with sensor attached such that pavement sample is exposed to direct sunlight.
5. Place sensor over a crack in the pavement sample.
4. Record measurements of crack location for 300 seconds.
5. Move the test apparatus with sensor attached such that pavement sample is in the shade. Do not move the sensor.
6. Record measurements of crack location for 300 seconds.
7. Return test apparatus and sensor so that pavement sample is exposed to direct sunlight.

8. Place sensor over a section of pavement not containing a crack.
9. Record measurements of crack location for 300 seconds.
10. Move the test apparatus with the sensor attached such that pavement sample is in the shade. Do not move the sensor.
11. Record measurements of crack location for 300 seconds.
12. Place the sensor over the sealed crack in the pavement sample.
13. Record measurements of crack location for 300 seconds.
14. Move the test apparatus with the sensor attached such that pavement sample is in the shade. Do not move the sensor.
15. Record measurements of crack location for 300 seconds.

4.4 - Results

4.4.1 - Data

Data was acquired per the procedures listed in Section 4.2. The data collected is contained in this section.

4.4.1.1 - Static Calibration Data

The data contained in Table 4.3 comprises the points which generates the calibration curve. This data is the crack position in millimeters sensed by the LSS as the local sensor was moved 2 mm perpendicular to the crack for each point.

4.4.1.2 - Precision Measurement Data

Three sets of 300 measurements of crack location have been collected to determine the statistical precision of the LSS. This data is plotted in Figure 4.4. The x axis corresponds to the sample number, while the y axis corresponds to the crack location in millimeters. Because the sensor was not moved during each of the three tests, the crack position determined by the LSS should not vary for each test.

4.4.1.3 - Performance Test Data

The LSS was placed over a crack and crack location was recorded for 60 seconds in both sunlight and shade. This test was performed over PCC and AC pavement samples. Over 1600 pieces of data for each test was collected in a 60 second period. The data is plotted in Figure 4.5, Figure 4.6, Figure 4.7, and Figure 4.8. The x axis corresponds to the sample number, and the y axis corresponds to the crack position determined by the LSS in millimeters.

KNOWN INPUT	OUTPUT 1	OUTPUT 2
38.000000	32.746662	
36.000000	32.746662	32.258759
34.000000	31.010548	31.905735
32.000000	30.890476	30.012257
30.000000	29.987213	29.987213
28.000000	28.233295	27.930908
26.000000	24.012699	24.012699
24.000000	23.843933	23.906847
22.000000	21.857887	21.763699
20.000000	20.144266	18.218100
18.000000	17.861162	16.001432
16.000000	13.968619	13.978721
14.000000	12.162083	14.129211
12.000000	10.076316	10.257970
10.000000	8.153798	7.973723
8.000000	6.113554	7.979305
6.000000	4.095878	6.087184
4.000000	3.822854	1.908245
2.000000	1.944149	0.006079
0.000000	-0.070333	-0.239264
0.000000	0.039217	-0.100104
-2.000000	-2.141565	-0.048830
-4.000000	-4.166034	-4.445074
-6.000000	-4.154767	-6.179636
-8.000000	-8.299613	-8.164840
-10.000000	-8.187638	-10.045124
-12.000000	-12.169043	-12.151710
-14.000000	-14.335826	-11.965364
-16.000000	-13.966684	-16.042248
-18.000000	-15.767681	-18.063887
-20.000000	-21.735266	-19.852913
-22.000000	-23.277716	-19.582764
-24.000000	-23.136930	-23.555916
-26.000000	-26.730637	-25.289291
-28.000000	-26.472023	-24.980011
-30.000000	-27.895861	-26.415539
-32.000000	-29.681419	-30.138300
-34.000000	-31.125687	-31.125687
-36.000000	-32.753983	-32.066742
-38.000000		-33.000137

Table 4.3 - *Static Calibration Data.*

4.4.2 - Results

4.4.2.1 - Static Calibration Results

Calibration procedure consists of determining output for a given input over the range of inputs which the instrument is to be used. This has been accomplished by comparing the response of the LSS to known input. From the calibration data, a calibration curve, or a plot of the instrument output versus the input over the usable range, has been generated. A best fit line has been fit to the data through the linear region of the plot using least squares method. The calibration curve is shown in Figure 4.9.

From this curve, the sensitivity, linearity, bias, and accuracy of the LSS has been determined. Sensitivity (also referred to as gain) or the slope of the calibration curve in the linear region, was found to equal 0.95020. The linear range of the sensor was found to be between -28 millimeters to +28 millimeters. In this region, the sensor output followed a straight line relationship to the input. It should be noted that the linear region is dependent on the field of view of the sensor and the width of the crack being sensed. See Section 4.5.1 for a discussion of the linearity of the sensor output. Bias, or systematic error, has been determined to be -.24725 millimeters. Finally, accuracy is the ability of the instrument to produce an output which corresponds to the true input. To quantitatively measure the accuracy, a percent error has been calculated. The value is expressed as a percent of the instruments full scale reading, using the point which strays most from the calibration curve. Percent error was found to be 4.29%. These results are summarized in Table 4.3.

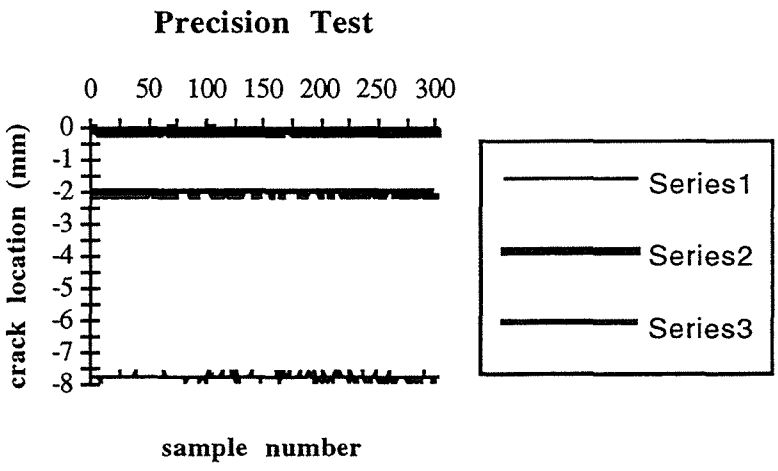

Figure 4.4 - *Precision Measurement Data.*

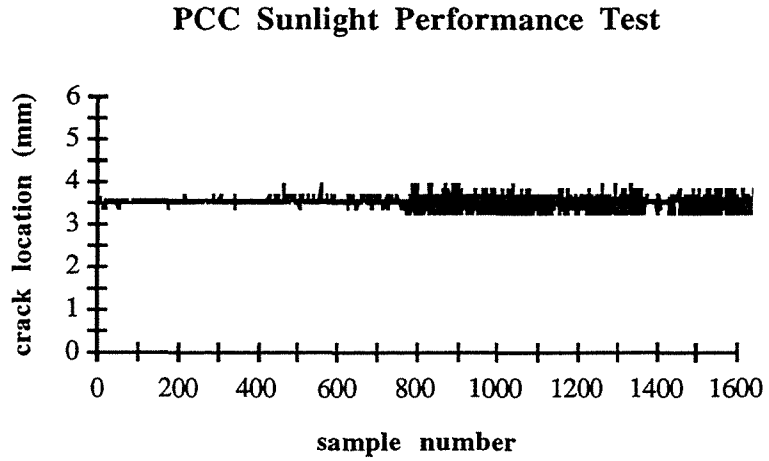

Figure 4.5 - *PCC Sunlight Performance Test Data.*

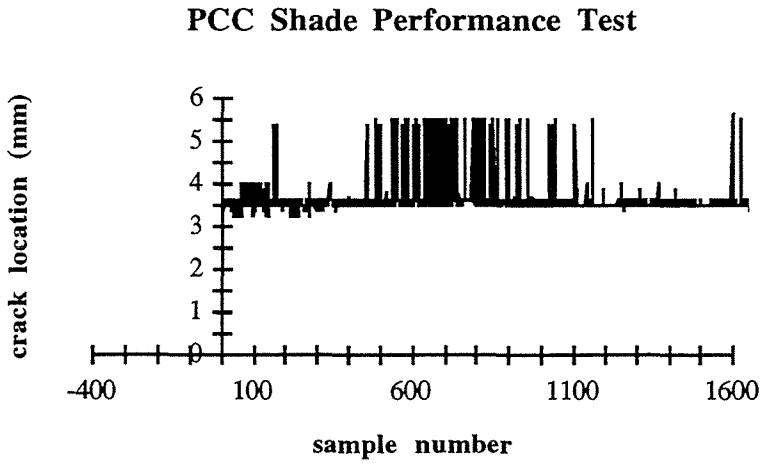

Figure 4.6 - *PCC Shade Performance Test Data.*

4.4.2.2 - Precision Measurement Results

Precision is defined as the ability of an instrument to produce consistent output for a given input. This has been determined by measuring crack location using the LSS and then statistically calculating the sampled standard deviation of the sample. A confidence level of 95% represents the probability that 95% of the measurements will lie within a given range. The 95% confidence range corresponds to +/- 1.96 times the sampled standard deviation. The 95% confidence level has been determined to represent the accuracy of the LSS. Average accuracy between the three tests was found to be +/- 0.114 millimeters.

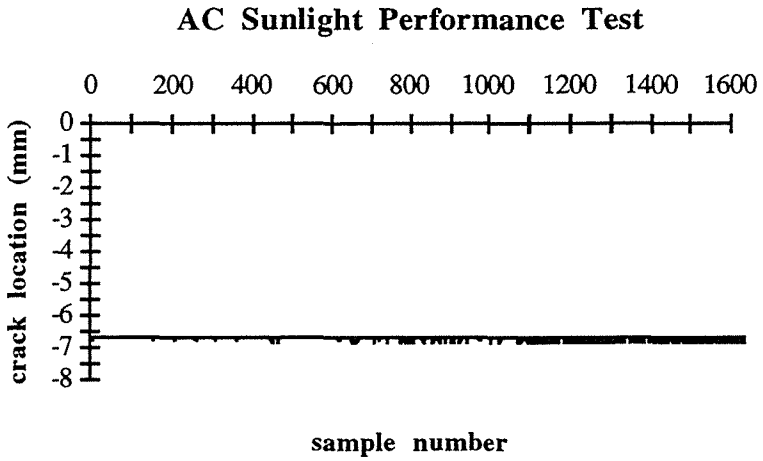

Figure 4.7 - *AC Sunlight Performance Test Data.*

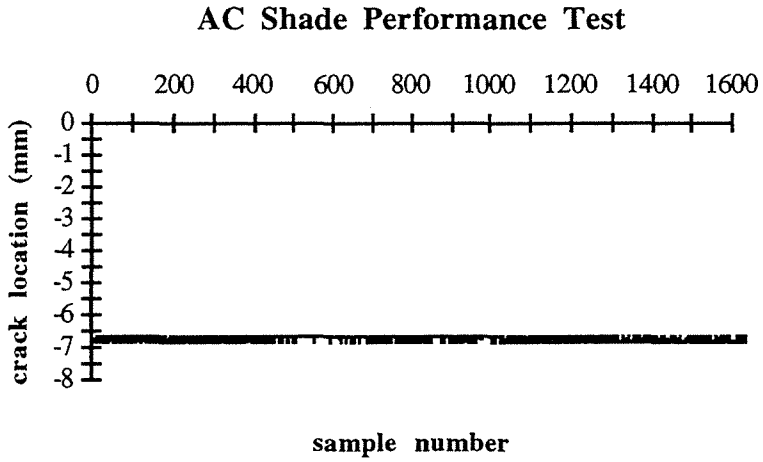

Figure 4.8 - *AC Shade Performance Test Data.*

SENSITIVITY	0.95920
LINEAR RANGE	-28 mm to +28 mm
BIAS	-0.24725 mm
ACCURACY (% error)	4.29% of full scale

Table 4.4 - *Static Calibration Results.*

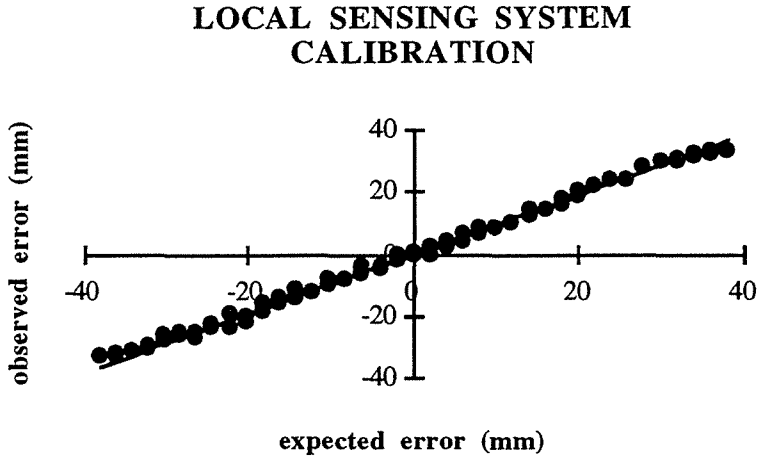

Figure 4.9 - *Calibration Curve.*

	AVERAGE	STANDARD DEVIATION	ACCURACY (95% confidence)
AC SUN	-6.727851	0.042584	+/- 0.083 mm
AC SHADE	-6.774620	0.070319	+/- 0.138 mm
PCC SUN	3.673418	0.506216	+/- 0.992 mm
PCC SHADE	3.543648	0.133550	+/- 0.262 mm

Table 4.5 - *Performance Test Results.*

TEST NUMBER	AVERAGE	STANDARD DEVIATION	ACCURACY (95% confidence)
1	-0.100873	0.059887	+/- 0.117 mm
2	-2.030466	0.055967	+/- 0.110 mm
3	-7.772348	0.059401	+/- 0.116 mm

Table 4.6 - *Precision Measurement Test Results.*

4.4.2.3 - Performance Test Results

The sensor must have the ability to distinguish between oil spots, shadows, previously sealed cracks, and actual cracks under different lighting conditions on both AC and PCC pavement. To ensure proper performance under these conditions, the

test procedure in Section 4.3.3 has been performed. To determine the accuracy of the LSS under these different conditions, a 95% confidence level has been calculated by determining the sampled standard deviation, as explained in the introduction to this chapter. Results are summarized in Table 4.4.

In addition to these results, the sensor consistently found no crack when the crack was located over a sealed crack in both shade and sunlight on AC and PCC pavement. Furthermore, the sensor never detected a crack when no crack was present in both AC and PCC pavement in both sunlight and shade.

Because the sensor location was not moved between the sunlight and shade tests for each pavement sample, the average crack location should ideally be the same for each test. For the test performed over AC pavement, the average crack location varied by 0.046769 millimeters while the crack location varied by 0.12977 millimeters over PCC pavement.

4.4.3 - Discussion

The objective of the experimental verification was to test the instrument response of the LSS. The instrument response is considered to be output produced for a given input. The input into the system is the absolute location of a crack in the surface being measured. The output of the system is the crack location generated by the LSS hardware and software. Additionally, the LSS must output a signal when no crack is located in the surface being measured. The LSS must produce viable output for all expected input under a variety of different operating conditions. This output must meet the requirements established in Section 4.2.

The first step in determining the system response was to perform a static calibration on the LSS. This was accomplished by comparing the response of the LSS to known input. From the calibration data, a calibration curve, or a plot of the instrument output versus the input over the usable range, was generated. A best fit line was fit through the linear region of the plot using least squares method. This curve is plotted in Figure 4.9 From this curve, the sensitivity, linearity, bias, and accuracy of the LSS has been determined. A problem arose in that the known input is considered to be the true input, while in reality it is affected by the response of the measuring instrument which is determining the input. In the calibration test, an Adept robot arm was used to position the sensor over the known location of the crack. The accuracy of the robot arm position is +/-1^{o} for each joint, and the corresponding arm lengths are 22 inches and 20 inches (Adept Technologies Incorporated, 1991). This corresponds to a worst case error of +/-1 inch when the joint angles are at 90°. The percent error

determined from the calibration procedure of 4.29% is considered to be primarily from the inaccuracies of the robot positioning system rather than the LSS. This conclusion is supported by the results of the precision measurement found in Section 4.4.2. The precision measurement results indicated that 95% of the crack location measurements should fall within +/-0.223 millimeters of the actual input. As seen by the calibration data in Table 4.2, the calibration data varied by a maximum of 2.3 millimeters. However, a 2.3 millimeter inaccuracy is still acceptable for the configuration of the Sealant Applicator System. As seen in Table 4.1, the sensor requirements specify a 2 inch (50.4 millimeter) allowable inaccuracy, so the LSS accuracy easily falls within the requirements established to achieve a proper seal.

Further error is caused by the fact that it is not physically possible to place the sensor exactly over the center of the crack at the start of the calibration procedure. This accounts for the bias error determined during the calibration procedure.

Ideally, the sensitivity of the LSS should be 1. However, the calibration curve revealed a sensitivity of 0.96. If a crack appeared at the end of the field of view of the sensor, a 1 to 1 relationship between the input and output would result in a crack location of 2 inches from the sensor (assuming a 4 inch field of view). A sensitivity of 0.96 rather than 1 would produce a crack location of 1.92 inches from the sensor. The 0.08 inch offset is negligible.

The results of the calibration curve showed a linear region of the input/output relationship to fall between +28 mm and -28 mm. The reason for the non-linear region is in the software. As the crack approaches the end of the field of view of the sensor, eventually the sensor will see the beginning of the crack but not the end of the crack. In software, the sensing system assumes that the end of the crack occurs at the end of the field of view, and calculates the width of the crack with this assumption. When less than 1/8" of the crack is contained in the field of view of the sensor, the LSS considers the crack to be too small to be sealed. Disadvantages in this algorithm are the inherent non-linearity which is produced at the ends of the field of view, and the fact that if a crack which is too large to seal only partially appears in the field of view of the sensor, the sensing system will not detect its entire width and will allow this crack to be sealed. Alternatively, when a crack only partially appears in the field of view of the sensor, the sensing system could ignore this crack because it cannot determine accurate crack location information. The effect of this would be to significantly reduce the usable portion of the field of view. For a 1 inch crack, the first and last 1 inches of the field of view would be ineffective. It has been decided that the disadvantages

associated with a reduced field of view are more detrimental than the disadvantages associated with non-linearities and inability of locating cracks which are too large.

During the calibration procedure, a crack which was 7/16 inch wide was being measured. When 1/8 inch of the crack remained in the field of view of the sensor, the LSS determined the crack location to be 1/16 inch from the edge of the field of view within the field of view. However, in actuality, the center of the crack was actually 3/32 inch outside of the field of view. This corresponds to a 5/32 inch (3.97 mm) error, which is apparent in the data gathered during the calibration procedure.

Maximum error due to the non-linearity would occur for the widest crack of 1 inch. When 1/8 inch of the crack remains in the field of view of the sensor, the crack position determined by the LSS will be 0.4375 inch (11.11 mm) off from the actual position. This error is still within the accepted accuracy of the LSS to achieve a proper seal.

During the performance tests, the crack location was sensed in both sunlight and shade over both PCC and AC pavement samples. The accuracies produced for the four tests, found in Table 4.4, all lie within acceptable tolerances of the system.

Furthermore, the LSS never mistook a sealed crack nor no crack to be a crack in the pavement. This was true over both AC and PCC pavement samples in both sunlight and shade.

4.5 - Conclusions

The Local Sensing System has consistently produced reliable and accurate results under a variety of operating conditions which fall well within the specifications established in Section 4.2. During the static calibration procedure, the accuracy, bias, sensitivity, and linearity of the LSS were determined.

The accuracy of the LSS was found to be 4.42% of full scale. It is believed that the majority of the inaccuracy is due to the robot positioning system which determined the input to the system, which was considered to be true. However, in reality the known input had a possible error of up to +/-1 inch. Still, the 4.42% error easily lies within the +/-2 inch accuracy required to achieve a proper seal.

The bias of the LSS was found to be -0.24725 millimeters. It is believed that this error is due to the fact that the sensor was not accurately placed over the center of the crack at the beginning of the procedure. This would account for an offset which is constant to all data collected. However, this bias is negligible in comparison to the requirements of the system established in Section 4.2.

The sensitivity of the sensing system was found to be 0.96, rather than a 1 to 1 relationship between the input and output. This creates a maximum error of 0.08 inch

at the end of the field of view, which is also negligible in comparison to the requirements established in Section 4.2.

Finally, the maximum error due to non-linearity in the LSS was found to be 0.44 inches. This would occur when a crack of 1 inch in width appears in the edge of the field of view of the sensor. This error is still well within the +/-2 inch accuracy necessary to achieve a proper seal.

The precision of the LSS was determined by taking a sample of data and determining the sample standard deviation. 95% of the data is contained within 1.96 times the sampled standard deviation. This 95% confidence was taken to be an indication of the precision of the LSS. The precision measurement results indicated that 95% of the crack location measurements should fall within +/-0.223 millimeters of the actual input. These results fall within the requirements established in Section 4.2.

The performance tests proved that the sensor produces reliable and accurate results under a variety of testing configurations which are expected to occur on the actual machine. The LSS never found a crack when no crack was present. Furthermore, the precision of the output over AC and PCC in both sunlight and shade fell within the requirements established in Section 4.2

5.0 - ROBOT POSITIONING SYSTEM (RPS)

5.1 - General Positioning System

5.1.1 - Introduction

Testing of control algorithms for the Robot Positioning System (RPS) were conducted using an Adept-3 manipulator. These tests were conducted in order to facilitate theoretical development of control algorithms while awaiting delivery of the GMF A-510 manipulator. The Adept-3 manipulator and the GMF A-510 manipulator are very similar in size and construction and have nearly identical kinematics. The GMF Karel controller and the Adept controller are also very similar. Special care has been taken to keep programming of the control algorithms as simple and as general as possible to allow for its portability between different industrial controllers.

An integrated force sensor was used for compliant motion control with the Adept-3. While a relative visual proximity sensor will eventually be used with the Local Sensing System (LSS), the algorithms for compliant control using force sensing and vision sensing are nearly identical. The force sensor was used to test control algorithms while the LSS was being tested and debugged. Later tests with the LSS concluded that the compliant motion algorithm will work with vision proximity sensing as well.

The objective of the compliant motion control algorithm is to establish a means of following a crack in the pavement using information from the LSS for closed-loop control. This can be accomplished by using the LSS mounted on the end effector to detect the displacement between the end effector and the center of the crack. This information can then be used to adjust the end effector trajectory to follow the path of the crack. This is an example of compliant motion control.

The purpose of the testing performed is to implement compliant motion on the Adept-3 manipulator using a visual proximity sensor. The compliant motion algorithm was developed for this project. The compliant motion algorithm developed will be used to follow cracks in highway pavement with a robot manipulator. The objective of the algorithm is as follows:

1) Use closed loop control with a visual proximity sensor to follow cracks in the pavement.
2) The only a priori information given will be the approximate starting orientation and location of the crack.

3) The algorithm must be implemented with closed-loop control in real-time.

4) Implement the algorithm using a standard industrial controller. This will allow the algorithm to be used with off-the-shelf components as opposed to custom built components.

A similar algorithm can be implemented using force sensing for compliant motion control. A desired contact force can be specified between the end effector and an object in the environment. Deviations between this desired force and the measured contact force are the force errors. These force errors are analogous to the displacements measured by the LSS. The force errors can be used to follow a contoured surface by 'feeling' the force the end effector is exerting on the surface and adjusting the trajectory. Thus, a compliant motion algorithm using force sensing can be ported to a system using a visual proximity sensor if the displacements read by the vision sensor replaces the force errors detected by the force sensor. The algorithm used is similar to the the one discussed by DeSchutter and Van Brussel (1988) except that position displacements are used in place of velocities. Position displacements are used because most industrial controllers are easily programmed for point-to-point position control and few controllers allow the user to specify velocity vectors. The algorithm is shown in the form of a flowchart in Figure 5.1.

5.1.2 - Algorithm Overview

Initially, the controller will be given information on the starting location and orientation of the path. The manipulator will then move tangential to the path and take a sensor reading to obtain its displacement from the center of the path. The sensor input will be run through a Proportional-Integral-Derivative (PID) control law to obtain a gain. This gain will determine how much the end effector should be moved in the direction normal to the path. The normal position gain vector will then be added the velocity gain vector which is paralell to the path. The two vectors added to the present location of the end effector will determine a new location in Cartesian space. This new location will be given to the motion controller which will move the manipulator in joint space. As the move is taking place, a new sensor reading will be taken and the next location calculated. For each move, a new end-effector orientation will be calculated by taking the difference between the present orientation and the estimated path direction. This difference will be run through a PID control law to obtain better dynamics. The end effector will then be rotated to the desired orientation for each move. The loop will continue until the controller receives a signal that the task is complete.

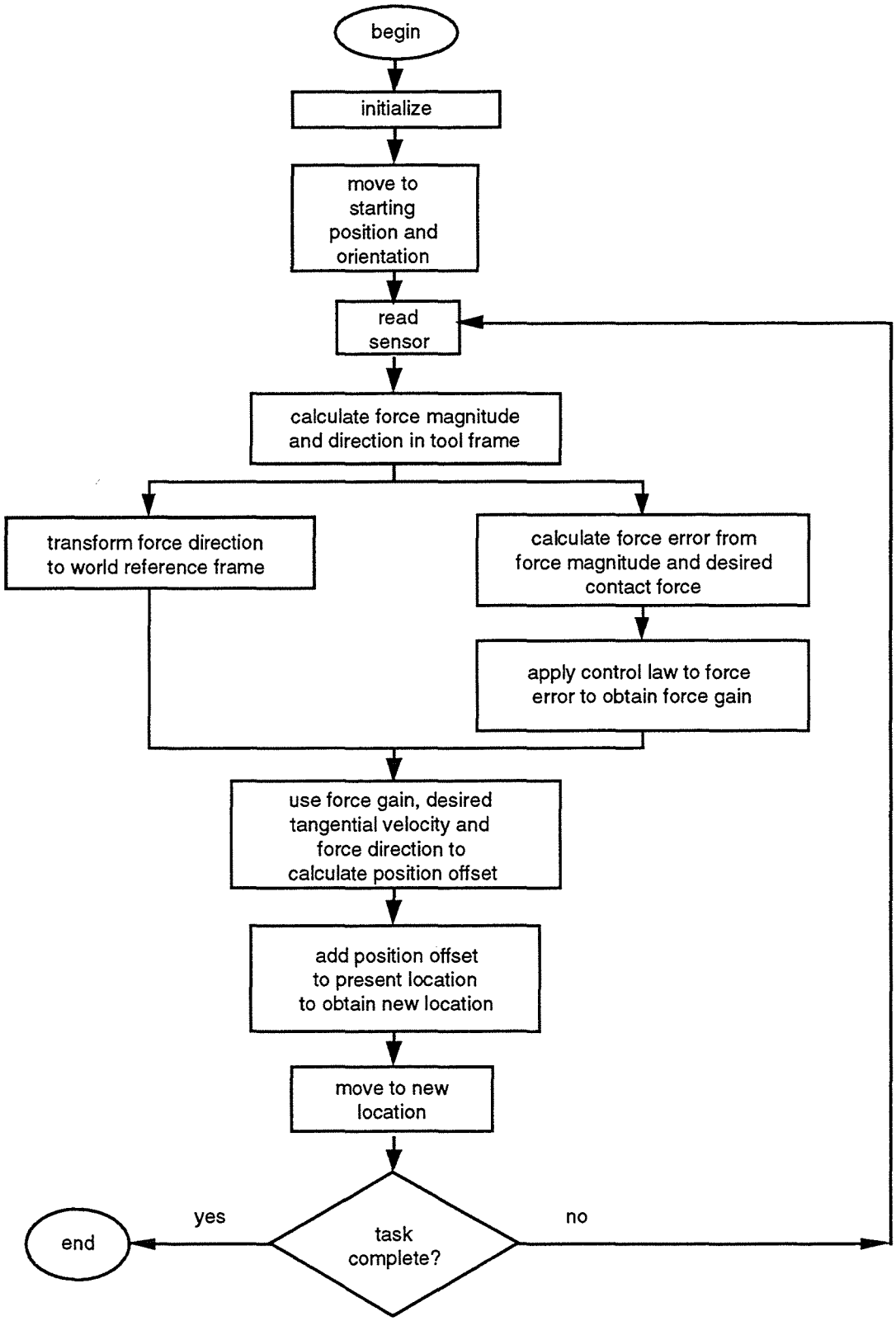

Figure 5.1 *- Compliant Motion Control Algorithm.*

5.1.3 - Measurement

At this point, it is important to note the differences between force sensing and the type of sensing being used with the LSS. Endpoint force sensing provides both the displacement of the end effector from the center of the path and the direction of the displacement. The displacement of the end effector can be calculated from the magnitude of the detected contact force and the estimated stiffness between the end effector and its environment. The direction of the applied force can be obtained from the components of force measured in the x, y and z directions of the tool frame. This type of sensing is used in the discussion given by DeSchutter and Van Brussel (1988). Absolute proximity sensing provides the displacement of the end effector from the center of the path measured along a normal to the path. Relative proximity sensing (as used by the LSS) returns a displacement from the end effector to the center of the path relative to the orientation of a one dimensional proximity sensor. Accurate sensing with a relative proximity sensor requires that the sensor always be aligned normal to the path being followed. The direction of the path being sensed with relative proximity can only be estimated indirectly. By using past Cartesian positions of the end effector along with the error measured at those points, the direction of the sensed path can be estimated. The accuracy of this estimation is dependent on alignment errors at the points being used, time delays in error feedback and other problems that can arise from discrete differentiation. While control with endpoint force sensing and relative proximity sensing are similar, relative proximity sensing introduces additional difficulties.

5.1.4 - Sensor-Controller Integration

Integration of the Adept controller with the PC used for processing sensor data is an important issue. Since the Adept controller and PC are equipped with serial ports, it was decided to use a serial link to pass the necessary data. For ease of communication, all displacement errors measured by the sensor were scaled and offset so that they could be transmitted as a single byte (decimal values 0-255). Additionally an extreme value (0 or 255) is sent if the crack is no longer in the sensor field of view. This makes the control algorithm more robust by allowing the controller to decide what to do if no data is available.

In order to be sure that all data received is current, a 'handshaking' protocol was implemented for serial communication. The controller transmits a byte over the serial port when it needs data and the PC sends the current error each time it receives a byte. The handshaking protocol can cause problems if one byte is lost because such

an event will stop communication altogether. It is also necessary to maintain a reasonably high transmission rate in order to obtain an update rate sufficient for real-time control. Ultimately, both the controller and the PC should utilize interrupt-driven serial communication software to assure guaranteed transmission. Presently an RS-232 protocol is being used. The PC does not use interrupt-driven communications software, but the problem of lost data has been temporarily averted by adding a buffer to the PC serial port.

5.1.5 - Results and Discussion

Results of the compliant motion algorithm using force sensing are shown in Figure 5.2. The significance of these results are that they prove the overall validity of the algorithm. Using the force sensor, the end effector is able to follow a surface while having no prior knowledge about the path to be followed. There is some error present in the trajectory of the end effector; however, these errors can be minimized by adjusting the control gains in the algorithm. The control gains were not adjusted so that more time could be devoted to implementing the control algorithm with the LSS. Also note that the path is not a perfect circle because the object deformed slightly due to the contact force from the end effector.

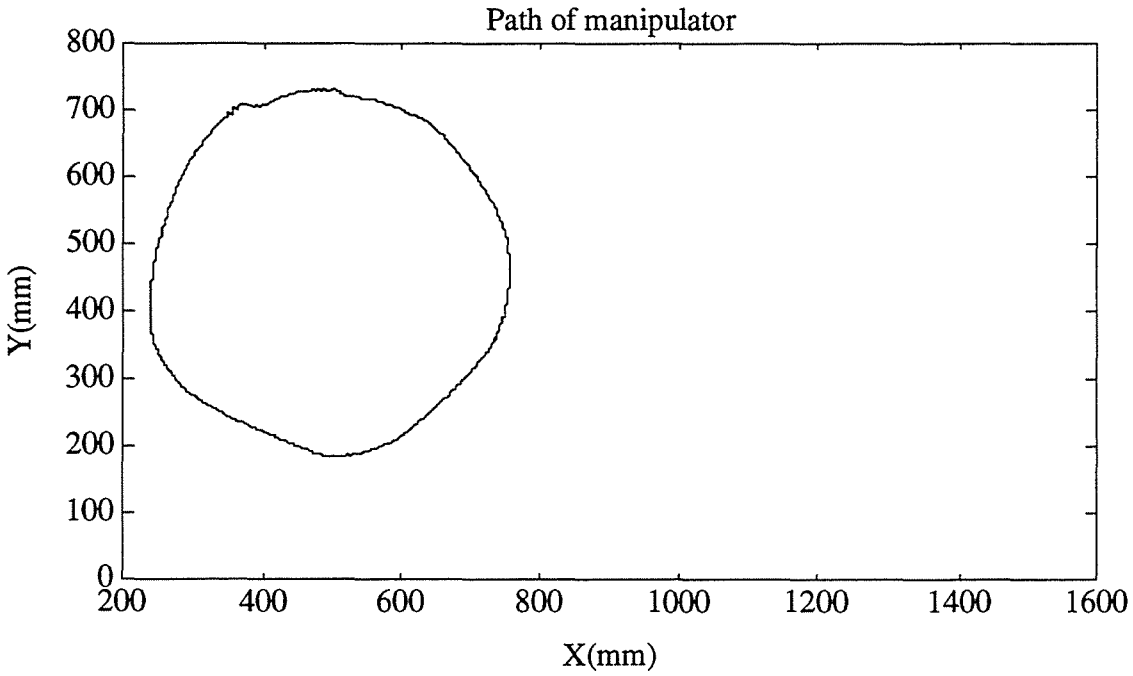

Figure 5.2 - *Cartesian path of the manipulator. The contour used was a flexible plastic circle 540 mm in diameter.*

Figure 5.3 shows a time history of the force error for the compliant motion algorithm. Note that there are several sharp increases or spikes in the values of the force errors. These spikes are disturbances caused by external factors. In this case the disturbances are caused by the end effector catching or sticking to the surface being followed. Note that once the disturbances are encountered, they slowly return to near-zero values. This is a result of the controller compensating for these disturbances. If the control gains are optimized, these disturbance will return to near-zero values in a much shorter time. The significance of Figure 5.3 is that it clearly shows the control algorithms accounting for disturbances from the environment. In the case of crack following, disturbances would include sudden changes in crack direction. The results from force sensing indicates that the control algorithm will be able to account for such disturbances.

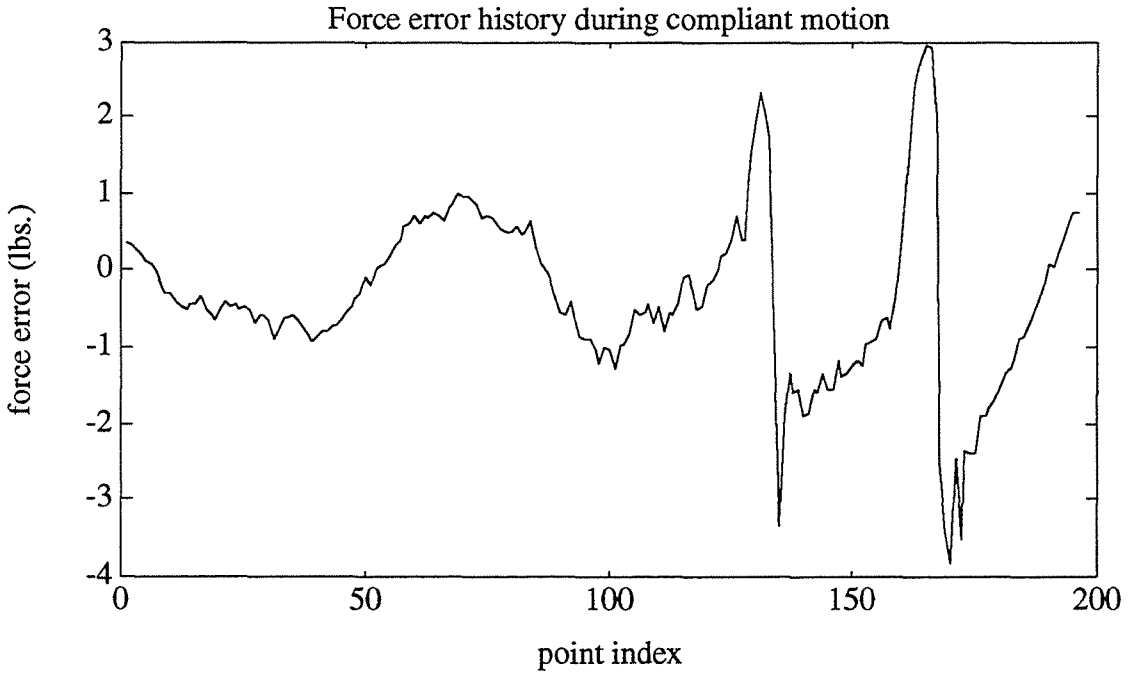

Figure 5.3 - *Error history during compliant motion with force control. The sharp disturbances were caused by friction between the end effector and the surface being followed.*

Data taken from test runs of the compliant motion algorithm using the LSS was used to create Figures 5.4 and 5.5. For the algorithm with the LSS, both the position and orientation of the end effector must be controlled. The time history of the position error is shown in Figure 5.5. The prominent "mound" in the center of the graph is due to a disturbance cause by the crack changing direction. Note that this disturbance is

gradually compensated for and the error returns to a near-zero value. The sensor has a field of view of approximately 75 mm which is much greater than any of the measured offset errors.

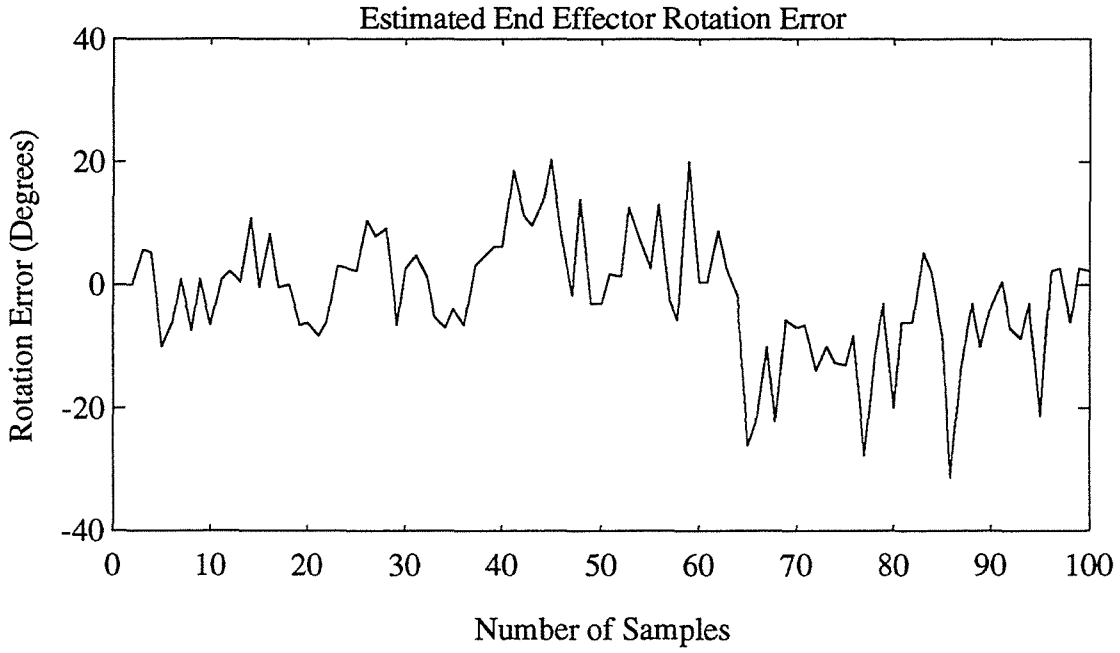

Figure 5.4 - *Sample of end effector rotation error. The rotation error is calculated from the estimated path direction compared with the actual end effector rotation. The run was approximaly 3 ft. long with a run time of 5 seconds.*

A sample of the time history of the orientation error of the end effector is shown in Figure 5.4. The algorithm was successful in controlling the orientation of the end effector in order to keep these errors sufficiently small. The control algorithm will work provided the orientation error is generally less than 30 degrees in magnitude. This condition is met in Figure 5.4. Results from the compliant motion algorithm using both the force sensor and the LSS indicate that crack following can be accomplished using a compliant motion algorithm as discussed earlier.

With the present algorithm, the controller receives the current position error from sensing system and processes the error in a PID control law in order to calculate the next position. System performance with this scheme is limited because most of the error information is never used. The algorithm was originally implemented with a sensor update rate of 4 Hz which is significantly slower than the controller cycle rate which varies between 4 Hz and 20 Hz. The sensor update rate was later improved by moving the software to a faster PC. With the improved update update rate (30 Hz),

system performance can be greatly improved by processing data as it becomes available and then updating the control algorithm with current filtered data as well as the integral and derivative of the error. Optimizing performance with this type of algorithm will require further research into the theory of control of discrete-time systems.

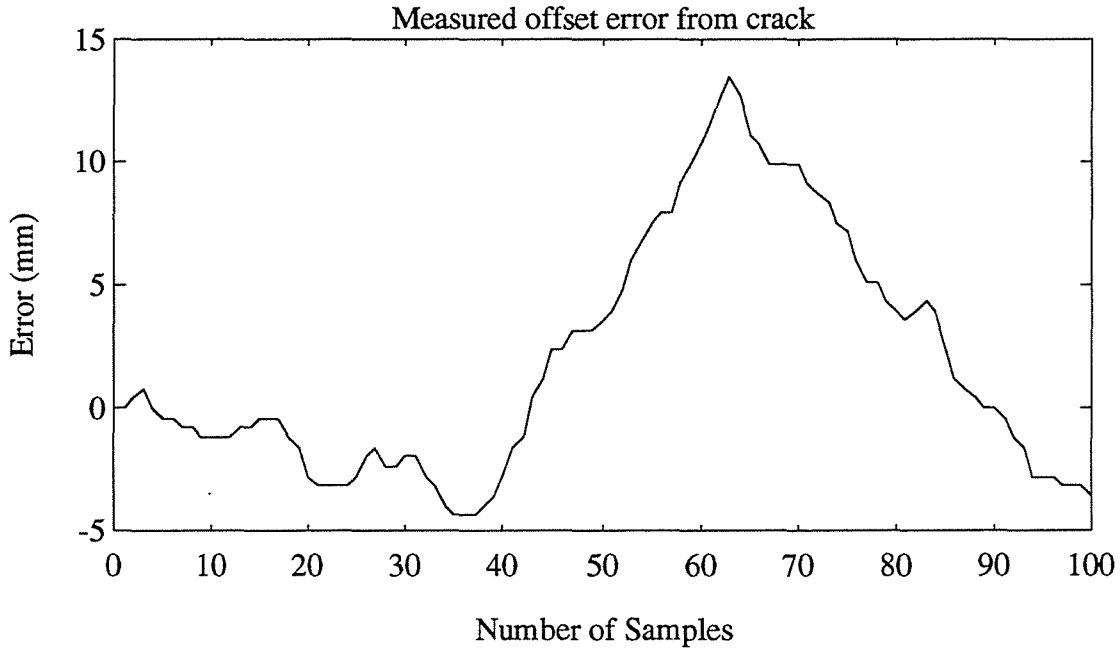

Figure 5.5 *- Measured offset error from crack for same run as above.*

5.1.6 - Conclusions

This section has described the theoretical basis for programming an industrial robot controller for compliant motion. The similarity between programming compliant motion using force and vision proximity sensor was explained. An algorithm was given for implementing compliant motion using a point-to-point industrial controller. The algorithm was first tested on the Adept-3 manipulator with a force sensor. The test with the force sensor was done while awaiting calibration of the visions sensor used by the LSS. An interface between a vision proximity sensor (the LSS) and the Adept controller was also tested preliminary to implementing compliant motion using the LSS. Compliant motion using the LSS along sample pavement cracks was tested. The results proved the validity of the control algorithm while showing the need for a more sophisticated algorithm to convert the sensor readings to control gains for the robot. The development and testing of these algorithms is targeted for their eventual

application in this project. Results of the tests that were done have also shown what work is necessary to improve the interface between the RPS and the LSS.

5.1.7 - Bibliography for General RPS

DeSchutter, J. (1990) "A Force Controlled Robot" in "Lecture Notes of the 1990 Integrated European Course in Mechatronics" "Computer Controlled Motion and Robotics" pp 213-230. Katholieke Universiteit Leuven, Department of Mechanical Engineering. Heverlee Belgium.

DeSchutter, J. (1990) "An Introduction to PID Control and Its Application to Motion Control" pp. 71-103. Ibid.

DeSchutter J. and H. Van Brussel (1988) "Compliant Robot Motion", *The International Journal of Robotics Research*, vol. 7, no. 4, pp. 3-32.

Luh, J. Y. S. (1985) "Design of Control Systems for Industrial Robots" Chp. 11 of *Handbook of Industrial Robotics*, John Wiley & Sons, Inc. Englewood Cliffs, NJ pp. 169-202.

Maciejowski, J. M. (1989) *Multivariable Feedback Design,* Addison-Wesley, NY. pp. 1-36.

Ogata, Katsuhiko (1987) *Discrete-time Control Systems*, Prentice-Hall, Englewood Cliffs, NJ.

Ogata, Katsuhiko (1990) *Modern Control Engineering*, 2nd. Ed., Prentice Hall, Englewood Cliffs, NJ.

Mason, M. T. and J. K. Salisbury, Jr. (1985) *Robot Hands and the Mechanics of Manipulation*, MIT Press, Cambridge, Mass.

5.2 - Longitudinal Positioning System

5.2.1 - Objective

The purpose of testing the longitudinal RPS mechanism was to verify the basic dynamic and structural capabilities and operating characteristics of the longitudinal machine without the actuator. The longitudinal RPS was developed in the second phase of the project to support testing of the Applicator and Peripherals System (APS) components and serve as a prototype of the machine to be used in Phase III. Delay in the delivery of the actuation system has caused testing of the complete longitudinal RPS to be postponed to Phase III. This report describes the results of testing of the longitudinal RPS without the actuation mechanism.

5.2.2 - Requirements

A. Function - The longitudinal RPS mechanism is required to support the APS components during operation and stowage. The APS components are the sealant applicator, heater/blower ducts, router with vacuum system and LSS sensor. These components are installed in the longitudinal machine cart and are modular in nature. In the extreme case, all the components listed are installed simultaneously (see Figure 5.6). During operation, the longitudinal machine provides a stable platform for the components which locate, prepare and fill the crack. It is designed to allow the actuator to move the cart laterally a total of 12 inches to automatically correct for the relative position of the crack with respect to the maintenance vehicle on which the LPS is mounted.

B. Operating Loads - Initially the cart was designed to carry the weight of all the components and the total weight of components was estimated to be 500 lb. The final design of the router component changed this requirement since the router is supported by its own casters and, when used with the longitudinal RPS, it supports the weight of the longitudinal cart together with the sealant applicator, the blower/heater duct and the LSS sensor (See Figure 5.6). The loads supported by the cart when operating without the router is now estimated to be 120 lb instead of 500 lb.

C. Stowage Loads - The load on the longitudinal machine during stowage and deployment is 500 lb since all the components are supported by the mechanism in this configuration.

D. Road speed - Operating speed of the machine is 2 mph with the router, and it maybe as high as 10 mph for the simplest operation, sealing only.

5.2.3 - Method

A. Test Hardware

- Longitudinal machine
- Sealant applicator component
- Caltrans test vehicle
- Router component
- Tools and equipment to support operation
- Video Camera

B. Facilities

- Road with AC surface on which routing and sealing operations can be performed.

C. Test Procedure

- Extend and retract cart with router and sealant applicators attached to verify stowing.
- Operate router and sealant applicator on actual roadway. Verify correct operation of longitudinal machine without actuator.
- When stationary, apply loads to cart on all three axes to investigate rigidity of the mechanism.

5.2.4 - Results

Proper extension and retraction of the longitudinal machine was verified with a 500 lb. load. A 2000 lb. winch was used to lift the unit at the center of the lower link and stowage was achieved in the configuration shown in Figure 5.7. The simple stowage design requires some manual manipulation of the cart as it is being extended toward the road. When the cart is lowered, to the ground, it is necessary to roll it outward manually once the casters touch the road. This allows the lower link to rotate parallel to the road. The geometry of the linkage is such that no manipulation is required when raising the cart and the links hang as shown. The winch raises the load to the stow position and once in this position the links are restrained with safety chains.

The longitudinal machine supported the operation of the router and sealant applicator as required. The router was operated at up to 2 mph and the longitudinal RPS mechanism resisted the reaction forces of router operation. No problems were evident.

A qualitative investigation of the rigidity was performed by applying loads to the longitudinal machine in the deployed position as mounted on the Caltrans test vehicle. Loads of approximately 100-200 lb were applied in the longitudinal and lateral direction of the cart at the hinge points with the lower link. The loads were applied with the table locked in the three positions representing the two extreme positions and the middle position of the 12 inch operating range. Testing showed that a significant portion of the deflection was due to movement of the bed and frame of the test vehicle. This made it difficult to obtain valid quantitative values representing the deflections of the longitudinal RPS by itself. It was evident that the longitudinal RPS base deflected when tested at the extremes of its operating range. The stiffness of the structure was determined to be adequate based on the initial investigation although increasing the stiffness of the base is recommended.

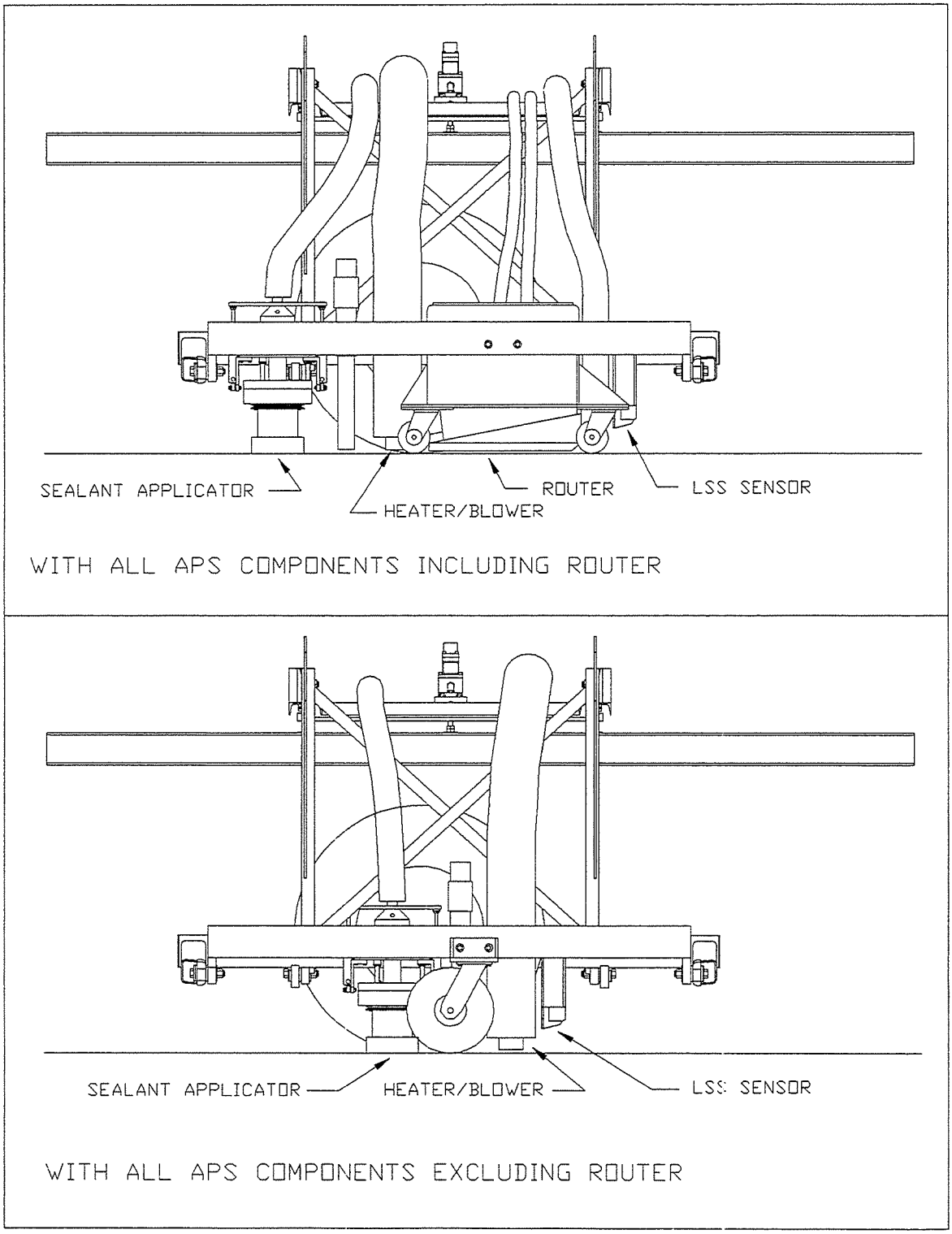

***Figure 5.6** - APS Components Installed in Longitudinal RPS.*

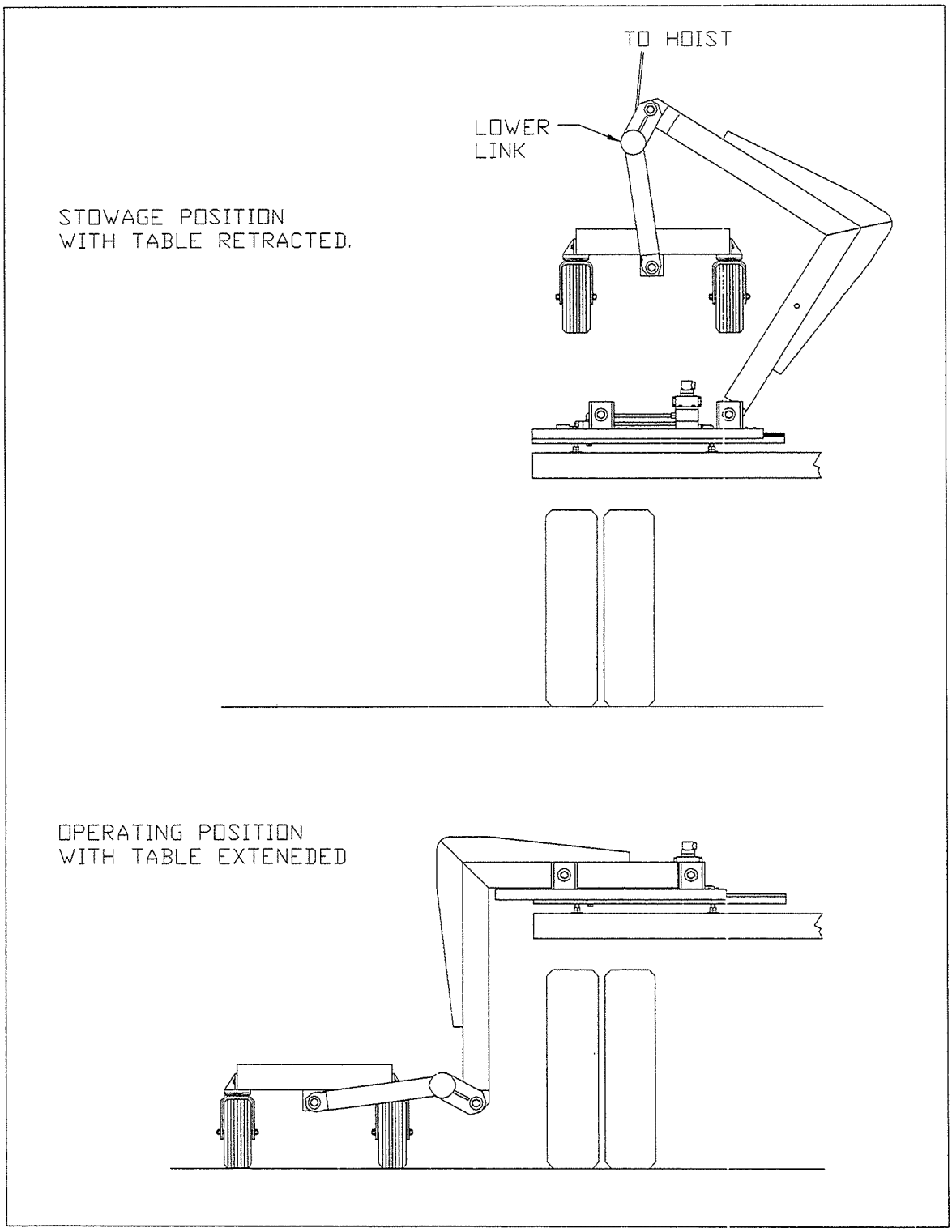

Figure 5.7 *- Operating and Stowed Positions of Longitudinal RPS.*

6.0 - APPLICATOR & PERIPHERALS SYSTEM (APS)

6.1 - Router

6.1.1 - Objective

Testing of the impact router was performed to evaluate its implementation with the crack sealing machine. The impact router was selected based on a review of available routing systems that are in use. Investigation and initial demonstrations of an existing commercial unit demonstrated that the design was compatible with the intended use on the crack sealing system. Testing of a manual commercial unit from Aeroil determined design requirements that were incorporated into the development of a router unit that could be integrated into the crack sealing machine. The resulting prototype was tested to verify functional characteristics.

6.1.2 - Requirements

The impact router must be capable of producing a rout configuration with a shape of .75 x .75 or a low profile rout. It must be capable of routing at surface speeds of 2 mph to support the longitudinal RPS and it must be capable of following general cracks that will be routed by the general crack sealing machine.

6.1.3 - Method

Testing was performed in two phases. The first phase involved testing of the manually operated Aeroil Router. The second phase involved testing of the APS router prototype which incorporated the basic impact routing design into a unit that can be used with either of the RPS systems.

Phase 1 -Test of Aeroil Router

Test Hardware

A. Aeroil Router Model #CJR24-6
B. Miscellaneous tools and equipment to support operation of router.
C. Video camera

Facilities

A. Road with AC surface on which routing is to be performed.

Method

A. Following operating instructions, operate Aeroil router to verify basic operating characteristics.

B. Evaluate router operation in forward and reverse directions.
C. Evaluate cutting speeds and cutting action.
D. Using resulting evaluation investigate the implementation of design changes that could improve operation.

Phase 2 -Test of APS Router prototype

Test Hardware

A. APS Router protoype
B. Caltrans test vehicle
C. Longitudinal machine
D. Hydraulic power supply
E. Miscellaneous tools and equipment to support operation of router.
F. Video camera

Facilities

A. Road with AC surface on which routing is to be performed.

Method

A. Mount router to the longitudinal machine and connect the hydraulic power supply.
B. Operate unit to verify basic operation
C. Evaluate operating characteristics of the router.

6.1.4 - Results

Phase 1-Testing of Aeroil Router

The Aeroil unit tested consisted of a cutting wheel powered by a 24 HP gas engine mounted on a cart with two wheels and a skid that acts as the third contact point to the road. The axles of the wheels are attached to the cart through linkages that allow the height of the cart to be adjusted. The cutting wheel is fixed to the cart and, therefore, the cutting depth varies as the cart is raised and lowered. An electric actuator operates the linkage and can be used to raise or lower the cutting depth during operation. The cutting wheel holds six rows of cutters and is designed to run at 2000 rpm. The cutters have a diameter of 4.75 inches and the total effective cutting diameter of the wheel is 15 inches. The maximum cutting width is 2.25 inches and the maximum cutting depth of the wheel is 1.25 inches. These dimensions are limited by the design of the cutting wheel. The operator, while walking backwards and pulling the machine, guides the unit by observing the cutting wheel as it follows the crack.

Debris is thrown in the direction away from the operator. This mode of cutting runs the cutter wheel in a "down-milling" mode (See Figure 6.1).

When operated in the normal operating direction, the router tended to pull itself up out of the road bed at higher surface speeds. Pushing the router results in a conventional "up-milling" cut (See Figure 6.1). Greater force was required to push the unit since the resulting cutting force acts in the direction opposite the direction of travel. The routing machine did not pull itself out of the roadway when pushed and it operated more smoothly. It was determined that operating the router in a conventional cutting mode was the most effective and would be used for the APS router.

As the router was operated at higher speeds, a significant amount of bouncing was observed. Design modifications were incorporated to limit the bouncing of the router and ease operation of the router during testing. The pneumatic wheels were replaced with solid rubber wheel of the same diameter. In addition, the third contact point, the skid, was replaced with a caster. These modifications reduced the bouncing of the unit significantly and the caster made it much easier to move the unit. Although the bouncing was significantly reduced the flexibility of the axle and linkage in the depth adjustment system was still contributing a significant amount to this problem.

During the testing the cutter wheels were worn and had to be replaced. The wear rate was significantly greater than expected and it was attributed to the attempts to operate at too high a road speed. It was determined that this problem would probably be alleviated by operating at a slower road speed, increasing the number of cutters, and increasing the rotational speed of the cutting wheel.

The APS router prototype design incorporated design constraints that addressed the results of the Aeroil router tests. The Aeroil cutting wheel was operated in the "up-milling" cutting mode. Rigidity of the unit was to be maximized. Rotational speeds of the cutting wheel were to be increased by selection of the appropriate hydraulic components.

Phase 2 -Testing of APS Router

The APS router component (Drawing SHRP(APS)RM-A100)is a modular unit that will operate in both RPS systems with minor modifications (See Figure 6.2). The unit consists of the Aeroil impact cutting wheel mounted into a frame supported on four casters. The cutting wheel is driven by a hydraulic motor with the lines running from the longitudinal machine cart to the power unit on the truck bed.

The cutting wheel and hydraulic motor are supported on a frame hinged on one end. This allows the cutter to be extended into the road and retracted using the same electric actuator installed on the Aeroil router test unit. The range of motion in the

present design allows for a cutting depth of up to .85 inches. The hinge point about which the cutter frame rotates is attached to an intermediate frame which is bolted to the wheel support frame. The intermediate frame also serves as the shroud and attachment point for the actuator and linkage. This results in a very compact self contained mechanism which is then mounted to the wheel support frame.

The linkage is designed so that at full extension of the actuator, the two links are in line with each other and the loads transmitted from the router cutting wheel to the intermediate frame will have no component in the direction of the actuator. The actuator will only be subjected to routing impact forces while it is extending the cutting wheel into the road and when fully extended the linkage acts as a rigid link. The hydraulic motor is keyed directly into the end of the shaft that drives the cutting wheel. The displacement of the motor is 1.95 cubic inches per revolution which is designed to have an output of about 17 HP at 2000 rpm with an input pressure of 2000 psi. The power for the test system is being provided by a hydraulic power supply acquired by other than SHRP funds. Operation of the router is achieved by powering the motor with the router retracted, then extending the cutting wheel into the ground to full extension while stationary. Once extended the router is moved forward to cut the channel.

During testing the router was set to cut a channel 1.25" wide X .5" deep to represent an intermediate configuration. The router was placed in the longitudinal machine and operated successfully. Because of limitations with the hydraulic power unit used to support the test, control of the router rotational speed was limited. The router was operated successfully at approximately 2 mph and wear of the cutter teeth was negligible when compared to the tests with the Aeroil router. Further investigation would be required to evaluate the long term relation of wear rate to operating speed. Results of the tests show that the requirements for routing with the general crack sealing machine prototype will be met with the APS router as designed.

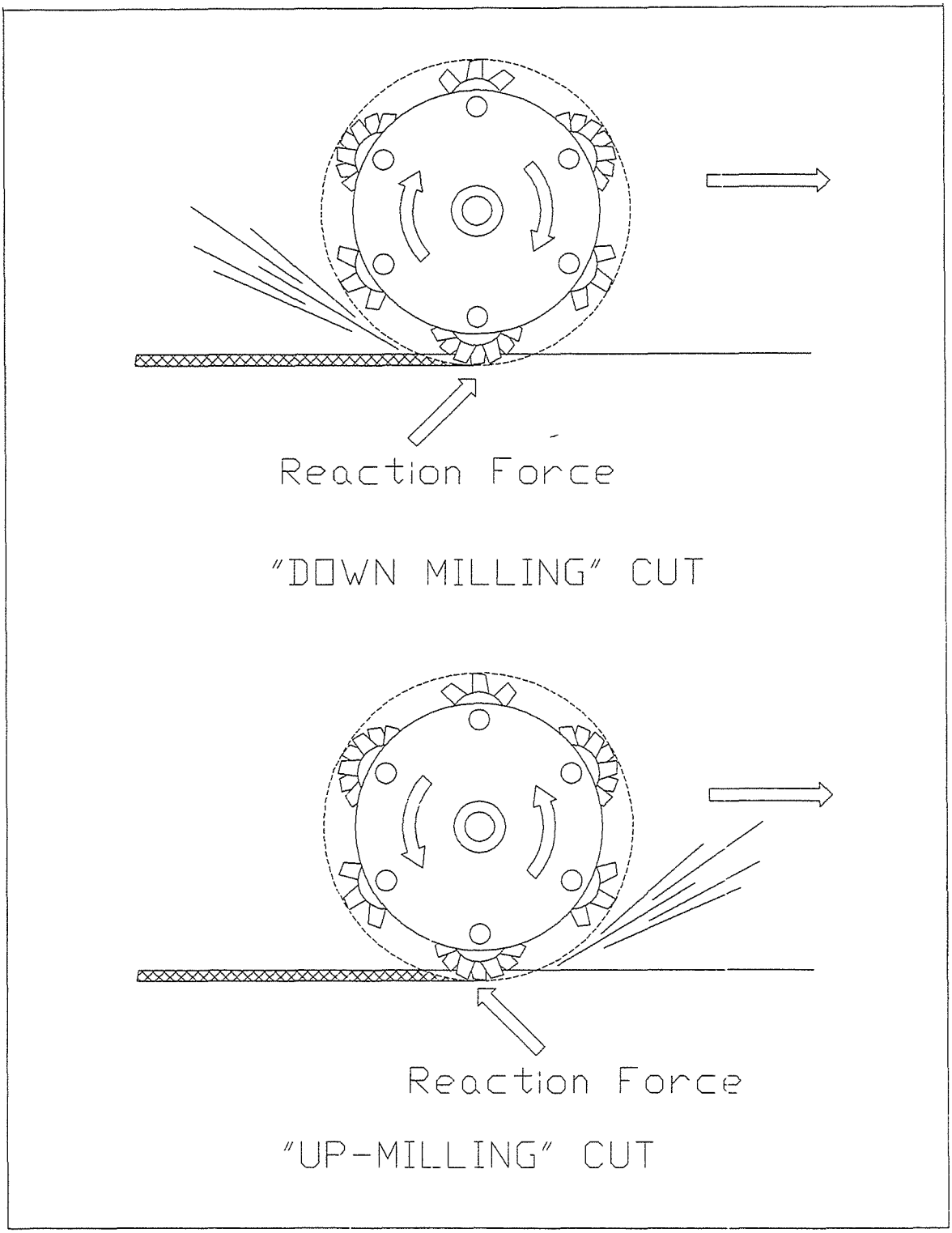

Figure 6.1 *- Methods of Material Removal.*

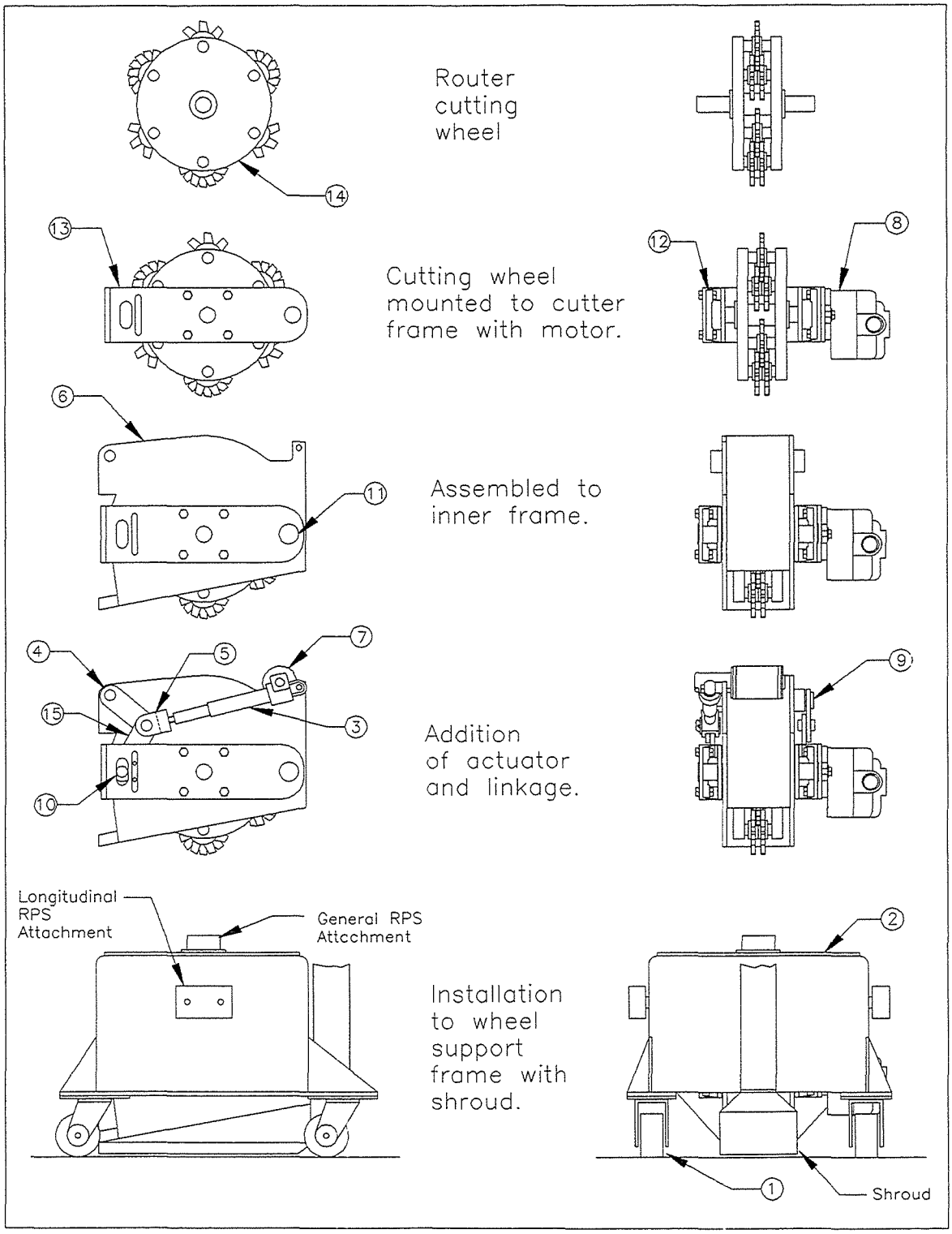

***Figure 6.2** - The Router Component.*

6.2 - Heating/Cleaning/Debris Removal

6.2.1 - Introduction

In this section, test results of the first generation Heating/Cleaning/Debris Removal System (HCD) components are presented. Primarily, the three main components of the system were examined separately. Since the debris removal unit is primarily an off-the-shelf industrial type vacuum with a custom inlet nozzle design, no tests during the component development portion of this project have been conducted. Instead, qualification testing of the unit integrated with the router will be conducted during the next phase, Phase III: component integration. Therefore, tests involving the cleaning and heating portions constitute the bulk of this section.

During the Phase I feasibility study, both radiant and convective off-the-shelf heating equipment was examined using the developed heat transfer models to determine a viable heating system for automated pavement crack repair. From the Phase I literature study and preliminary component testing, it was determined though, that for this project, the most feasible means of *cleaning* pavement cracks automatically is by using high volume air from a centrifugal blower. Therefore, in determining which equipment to test, it was apparent that a convective heater could dually serve as a crack cleaning and heating method. Therefore, this type of equipment was concentrated on during testing.

Before discussing the testing, a crucial design issue must be resolved, the desired crack temperature before sealing. Currently there is no conclusive evidence dictating optimum crack surface preheat temperature. Road crews today currently heat cracks until the surface begins to smoke and discolor. They then typically follow some time afterwards applying sealant. This delay between crack heating and sealant application often approaches several seconds thereby allowing the crack surface time to significantly cool (see Figure 6.10). By permitting the crack to cool, the freshly applied, 425°F sealant sets up quicker, inhibiting good sealant flow into the crack. Therefore, the heating done to enhance sealant quality is often partially negated by delayed sealant application.

Through automation, a goal of the crack sealing project is to shorten this delay by minimizing the time (or distance) between heating and sealant application. This will help ensure adequate sealant flow into pavement cracks. Yet, the temperature of the optimum surface preheat is still unknown.

A brief investigation was conducted by UC Davis crack sealing project personnel to estimate the temperature at which AC pavement discoloration begins. Through the

use of a hand held infrared measurement device, this temperature was estimated to be 280°F. This seems reasonable since other researchers (see Phase I Final Report) determined that AC pavement combusts at 350°F. Therefore, in the interest of safety and a quality seal, it was decided that a conservative surface temperature goal of 250°F be adopted in developing the heating unit. At such a temperature, moisture should be evaporated and sealant flow should be much enhanced compared to current sealing methods.

6.2.2 - Convective Heating Tests

Convective heating as a crack heating method appears, immediately to have one advantage over radiant. The exhaust gas from the heater could dually serve as a means to heat *and* clean the pavement cracks, as in the HCA lance. This could add to the compactness of any heating system. In order to test such a commercially available convective heater and thereby implicitly verify the validity of the convective model, it was first necessary to construct a test apparatus.

6.2.2.1 - Set-up

To best simulate the relative motion between the vehicle and pavement surface, a movable test apparatus was built. The top portion was made from steel channels to serve as rails upon which a motorized cart containing the propane heater could ride. This cart could then be moved across the asphalt sample, heating its surface as it passes by (see Figure 6.4). As can seen from Figure 6.3, an infrared pyrometer was used to continuously measure the surface temperature of the sample just after the heater is passed over. This method of temperature measurement was chosen since a real-time, non-tactile means of measuring pavement temperature would most likely be necessary on the final cleaning/heating system. Also, a pyrometer provides a means of averaging the temperature variations, inevitably present from point to point on the non-homogeneous pavement surface, over the region of interest. It does this by measuring the total heat seen through its lens and dividing it by its focal area. While a matrix of thermocouples placed at various depths in the sample are very inexpensive and have been used in studies previously, the tiny 0.005" diameter K-type thermocouples needed to meet the quick response requirements (less than 100 ms) for this application proved to be very fragile and electrically noisy for the data acquisition hardware in use (see below). As such, thermocouples were discarded as a viable test measurement device. While thermocouples do appear in some of the photos that follow, their outputs were not used in analyzing any of the test data. A pyrometer is generally very accurate and quick, yet is much more expensive.

The pyrometer purchased is a Raytek Thermalert ET3LT. It features adjustable emissivity, 12 bit digital circuitry, and outputs a standard linear 4-20 mA control signal representing a surface temperature between 0 and 400°F. For this temperature range, this means a resolution of roughly one 0.1°F can be achieved. It has a 95% response time of 80 ms (2.88" of pavement surface at 2 MPH). Also, the water cooled housing and air purge collar options were purchased to keep the circuitry cool and the lens dust-free in a harsh environment. To continually store the pyrometer surface temperature readings as the heater is passed over the sample, a Microsoft QuickBASIC program was developed using a DAS-16 data acquisition card from Keithley/Metrabyte (program code available upon request).

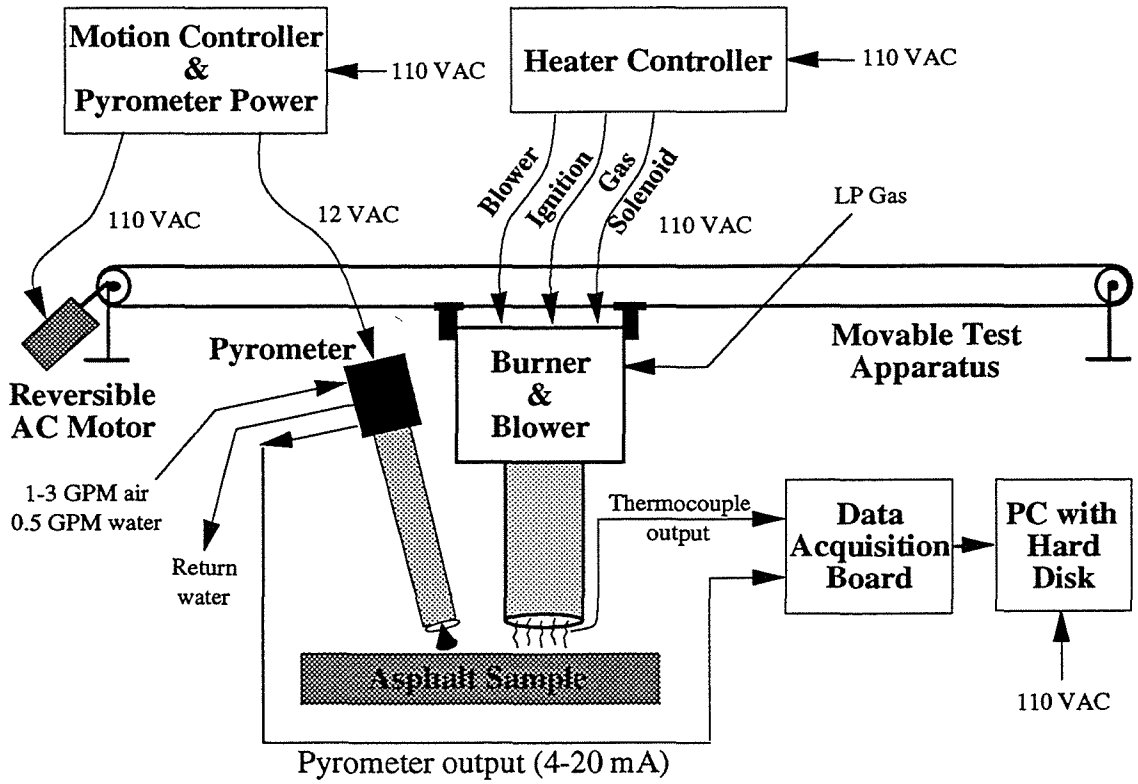

Figure 6.3 - *Experimental set-up.*

A commercially available burner was then needed to attach to the test apparatus. Using the convective heat transfer model, a burner system able to heat the surface of the roadway as close to 250°F as possible while passing by was sized. It should be noted that burner size is not directly proportional to vehicle speed. This is because heat can only be transferred to the surface of a medium via the local heat transfer coefficient which, as shown in the March 1992 interim report, is a non-linear function of

Reynolds number or, more specifically, exit diameter. Thus, a large BTU rating coupled with a small exit diameter provides the best heat transfer.

It was desirable to maximize the heat transfer and automation of the heating process. Vendors were contacted and various burner configurations were examined. It became apparent during this process that to achieve a surface temperature of 250°F at 5 - 10 MPH would require an expensive, inefficient, noisy, and cumbersome heating system. Keeping in mind the scope of this project, to produce prototype crack sealing machinery that can be used in developing a machine for later commercialization, smaller, more reasonably sized burners and burner control systems were therefore looked at that, during commercialization, could be replaced with a larger unit.

The choice was made to test a 1.8 million BTU/hr tube burner by Sur-Lite Corporation because of its high convective heat transfer ability and small size. It was estimated, using the computational model, that a surface temperature close to 250°F with a relative speed of 2 MPH could be attained with a slightly modified stock unit. The standard stock unit uses air from an onboard 300 SCFM blower mounted to the burner to produce an exit velocity estimated to be 35 MPH from its 6" diameter flame tube. It was felt that by necking down this exit tube to effectively create a nozzle, the exit velocity could be greatly increased, perhaps to over 100 MPH. However, to do so, the standard 1/3 HP, low pressure blower (less than 1/4 PSI) must be replaced with an optional 3-phase electric or hydraulic high pressure blower (approximately 10-15 HP, 2-4 PSI) which would be better equipped to handle the associated pressure losses that accompany the addition of a nozzle. The Sur-Lite system comes as a complete integrated package and is therefore more reliable than a currently used hand held HCA lance. A flame safeguard system is provided which includes automatic ignition, throttling, shut-down, and emergency shutdown.

Sur-Lite was contacted and a standard low pressure tube burner, model 12031-4, configured with a *low* firing fuel train was sent to UCD on loan. While if given the choice, a fully equipped, high firing unit with an optional hydraulic high pressure blower would have been tested, Sur-Lite personnel were kind enough to loan their equipment for the study. The test results therefore reflect the significantly low heat output of the burner (approximately 200,000 BTU/hr) and low burner exit velocity (approximately 35 MPH) associated with the large 6" diameter exit. For purposes of these tests and comparison with the heat transfer model though, these factors were not important.

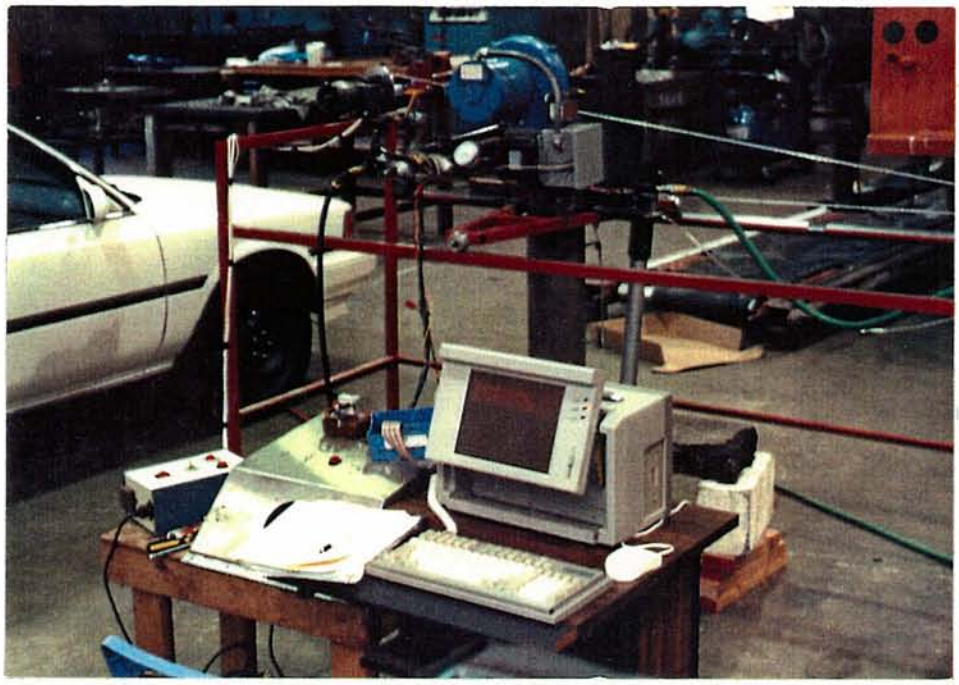

Figure 6.4 - *Test apparatus set up with Sur-Lite burner installed.*

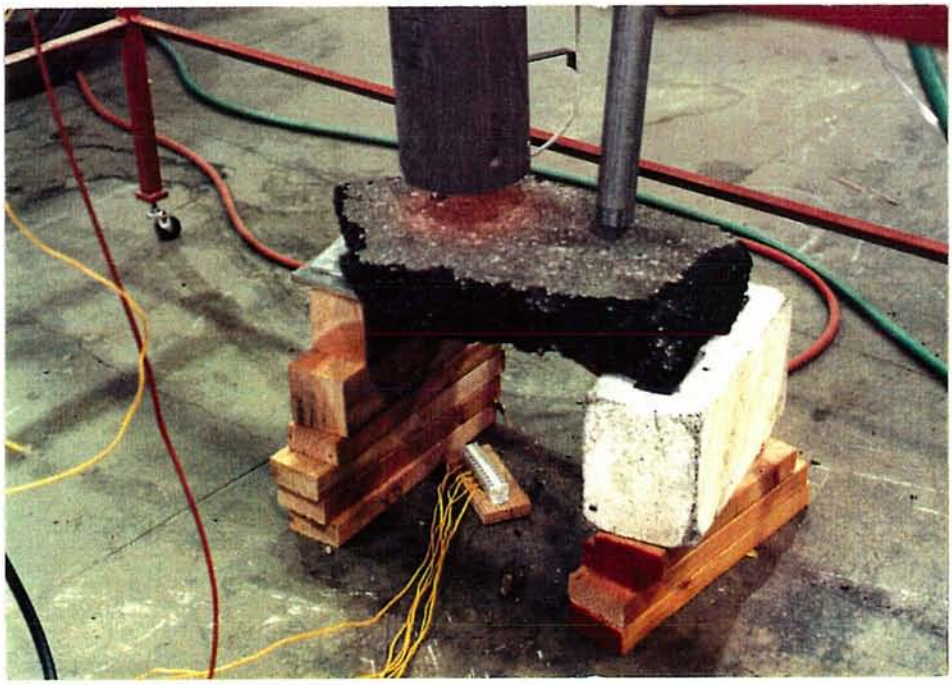

Figure 6.5 - *Close up of sample being heated with Sur-Lite burner. Note: the thermocouples mounted in the sample were not used in this study.*

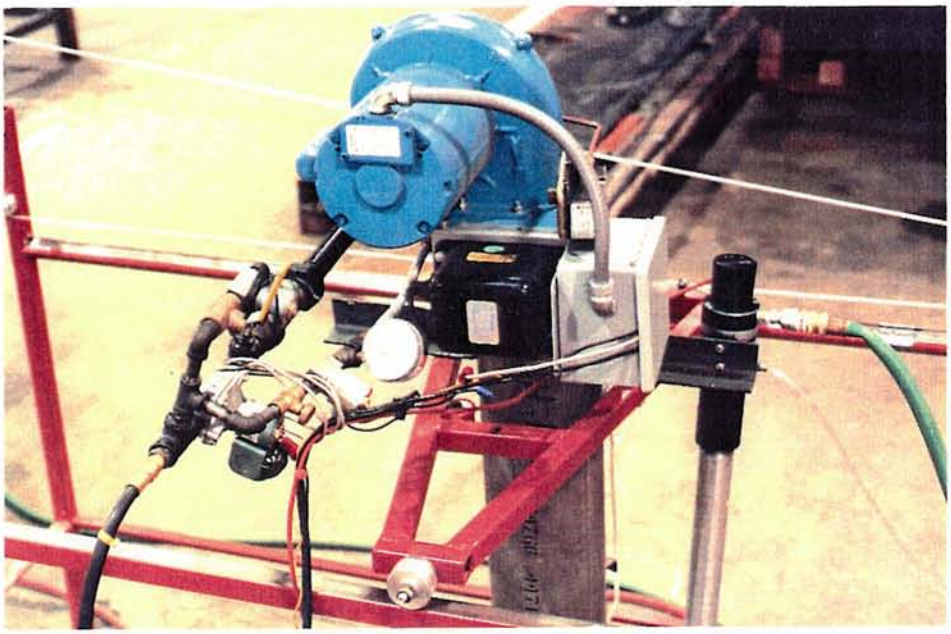

Figure 6.6 - *Sur-Lite Burner with Raytek pyrometer mounted adjacent. Note the water cooled housing and air purge attachments on the pyrometer.*

Figure 6.7 - *Data acquisition station. The control box on the left provides power to the cart motor. To its right is the scrap panel that houses the spark ignitor push button and solenoid valve toggle switches for the burner. On top of it is the transformer providing 12 VAC power to the pyrometer and the connector board for the inputs to the DAS-16 card. On the floor a thermocouple is connected through a DVM to measure ambient temperature.*

The borrowed Sur-Lite heater thus described was then mounted on the test apparatus described above, wired through a scrap bench test control panel, and tested against model predictions (see Figures 6.4 - 6.7). As seen in these figures, a K-type thermocouple was placed in the center of the exit stream at the end of the burner tube, approximately 1" from the pavement in most cases. This was done to record the temperature of the impinging air flow for later entry in the software model.

6.2.2.2 - Procedure

To best compare temperature profile data from the convective model with data gathered testing the Sur-Lite burner, a formal test procedure was adopted. Test runs were typically performed as follows. First, the ambient temperature was measured using a cold-junction compensated, K-type thermocouple device connected to a digital voltmeter and entered into the data acquisition program - and later in the heat transfer model. Next, the height of the burner, sample number, and pyrometer location (distance aft of duct) were recorded. Third, with the heat off, the cart was rolled across the sample at a constant rate (determined by measuring the time taken to cover the test section distance of 62") while collecting surface temperature data. The heater was then ignited and allowed to warm up for several seconds. Then, again with the computer acquiring surface temperature data, the heater was passed over the sample. The surface was then allowed to cool before the next run. These steps were repeated with varying speeds, samples, fly heights, and exhaust temperatures (a function of LP gas pressure).

During each run, the DAS-16 QuickBASIC program recorded to disk, the heat source temperature according to the thermocouple located at the tube exit, and the surface temperature that the pyrometer encountered based on its .95 emissivity setting. Since the data collection program had to be started before the heater was passed over the sample, to capture the entire run, it was useful to develop a method of flagging the data so as to not analyze data that was not of interest. This was accomplished by placing aluminum plates at the both ends of the AC sample. Since, the pyrometer measures reflected infrared energy using emissivity in its calculation to solve for temperature, a drastically incorrect reading is recorded when it comes across a substance with an emissivity that does not match that which it has been set for. In a test run data file this shows up as a spike in the temperature. Therefore, only the data between the two flags or spikes in the file is of interest for analysis.

6.2.2.3 - Analysis

Following the above described test procedure, 30 tests using the Sur-Lite burner were conducted. For each test, a data file containing pavement sample surface temperature and burner exit temperature at each sampling time was stored on disk. These files were then transferred to spreadsheet file format in order to graphically compare the results to those predicted using the model.

To compare the surface temperature data gathered from each of the test runs to the surface temperature predicted using the convective heat transfer model, the sampling frequency, average source temperature, cart velocity, ambient temperature, and initial surface temperature, had to be entered as parameters to the model. After entering those values, specific to a given test run, into the model's input file, the model was run and an output file was generated.

The output file created by the model contains the predicted surface temperature at each time step in the heater's journey across the pavement sample. More specifically, the model predicts the temperature that a specific point on the surface of the sample should experience as the heater is passed over it using the equations developed during Phase I and presented in the March 1992 interim report.

As explained, the model forecasts the temperature history of a specific point on the sample's surface. However, during the tests, the surface temperature was sampled continuously as the heater was passed over the sample. So, to graphically compare the continuously measured temperatures to the model's single predicted temperature, the measured temperature was plotted as a function of time and the predicted value was shown as a horizontal line across the graph. To attain a reasonable first order comparison between the two, the average of the surface temperatures measured between the spikes or flags was also calculated and shown. A plot of a representative run is thusly shown in Figure 6.8. Plots of 28 of the 30 tests can be found in the March 1992 interim report (tests #1 and #6 were conducted in error).In plotting the test data, the model's predicted temperature had to be corrected for the location that the temperature was measured at during the tests, i.e., the location of the pyrometer aft of the centerline of the burner. The distance was measured and divided by the cart velocity to determine the time taken to cover that distance. This time was then added to half of the total predicted time (to account for the heating that took place as the cart approached) to arrive at the total exposure time. The temperature at this time in the output file was taken as the predicted temperature and plotted in the comparison charts. As can be seen, the surface temperature predicted by the model compares reasonably well to that actually measured.

AC Pavement Temperature History

300 CFM Sur-Lite Burner - Test #13

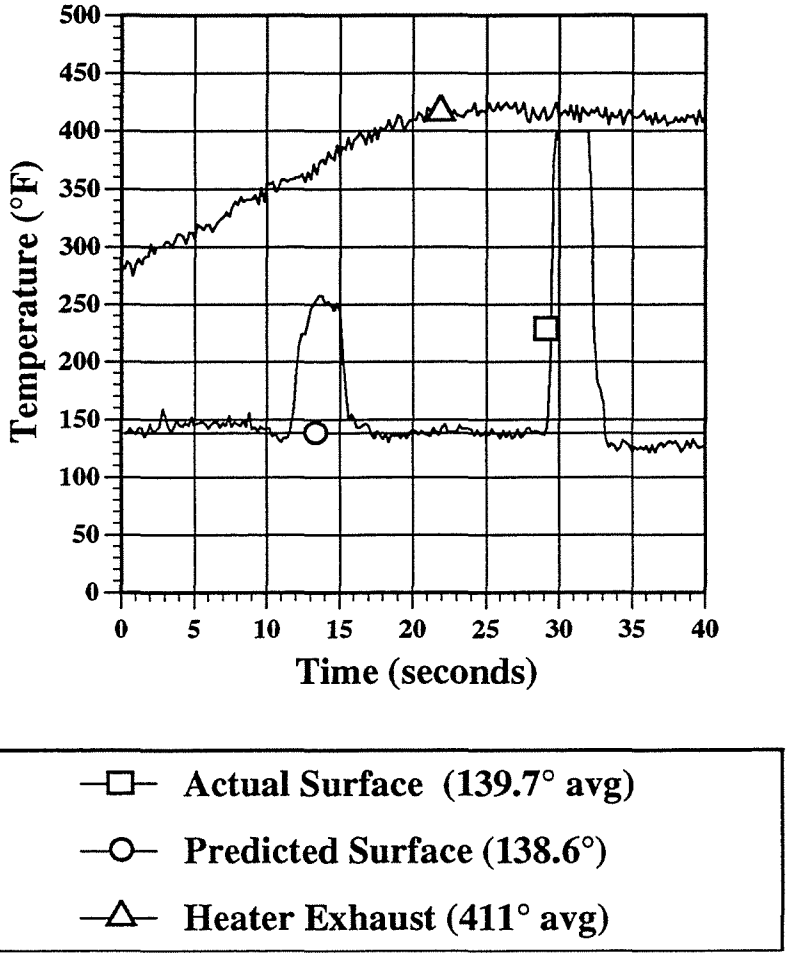

Figure 6.8 - *Sur-Lite burner test #13. Note the flags (spikes) in the data representing the beginning and end of the pavement sample. The average temperature calculated was based only on the data between these spikes.*

It should be noted that test runs 25-30 were designed to examine the ability of the model to predict pavement surface temperature under longer heat exposure. This was accomplished by slightly modifying the convective FORTRAN model to accommodate a stationary heater, i.e., setting *r/D*=0 and applying heat for 2-5 minutes while acquiring surface temperature measurements. Due to the physical limitations of the test apparatus though, it was impossible to measure the temperature of the pavement surface while it was being heated (see Figure 6.5). But, the pyrometer could be moved

AC Pavement Temperature History

300 CFM Sur-Lite Burner - Test #27

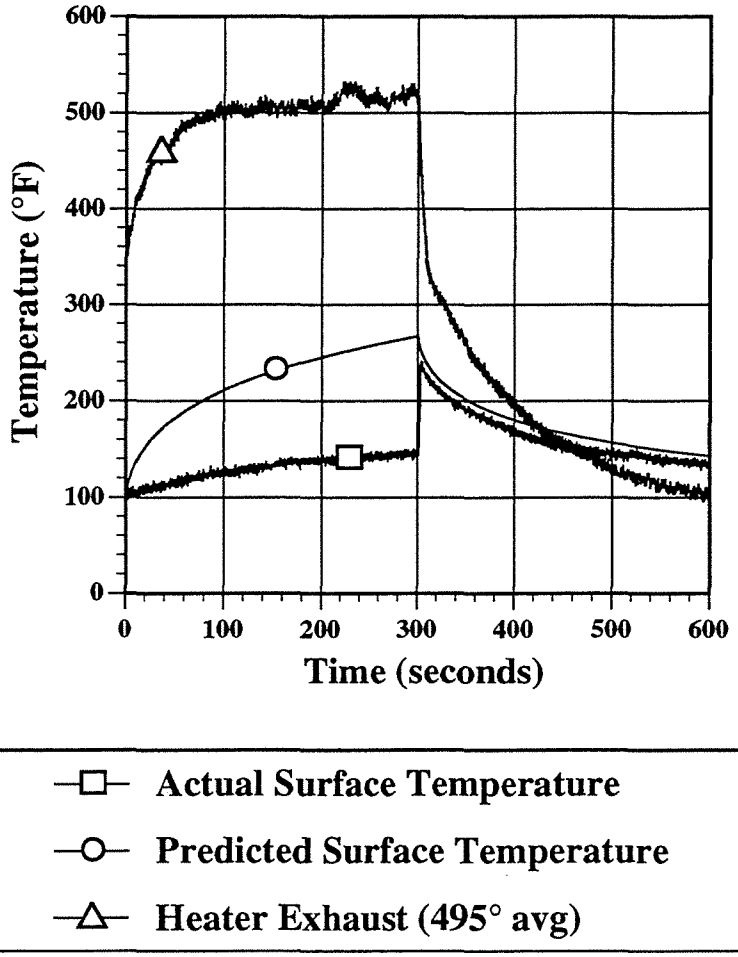

Figure 6.9 - *Sur-Lite burner test #27 (long exposure run). Note the low actual temperature measured during the first half of the run. This is because, during the first 300 seconds, the pyrometer was not aimed at the sample being heated - due to its position aft of burner. After turning off the heater and moving the pyrometer over the hot sample, the actual surface temperature is registered. The average source temperature used in modeling the run is based on the first 300 seconds of data.*

over the heated section just after removing the heat to monitor the sample while cooling. It was felt that if the cooling curves of the experimental and predicted approximately matched, it would be reasonable to assume that the surface was heated to roughly the same temperature and therefore, that the model does adequately

predict surface temperature under longer exposure. As can be seen in Figure 6.9, the predicted and measured cooling curves do compare reasonably.

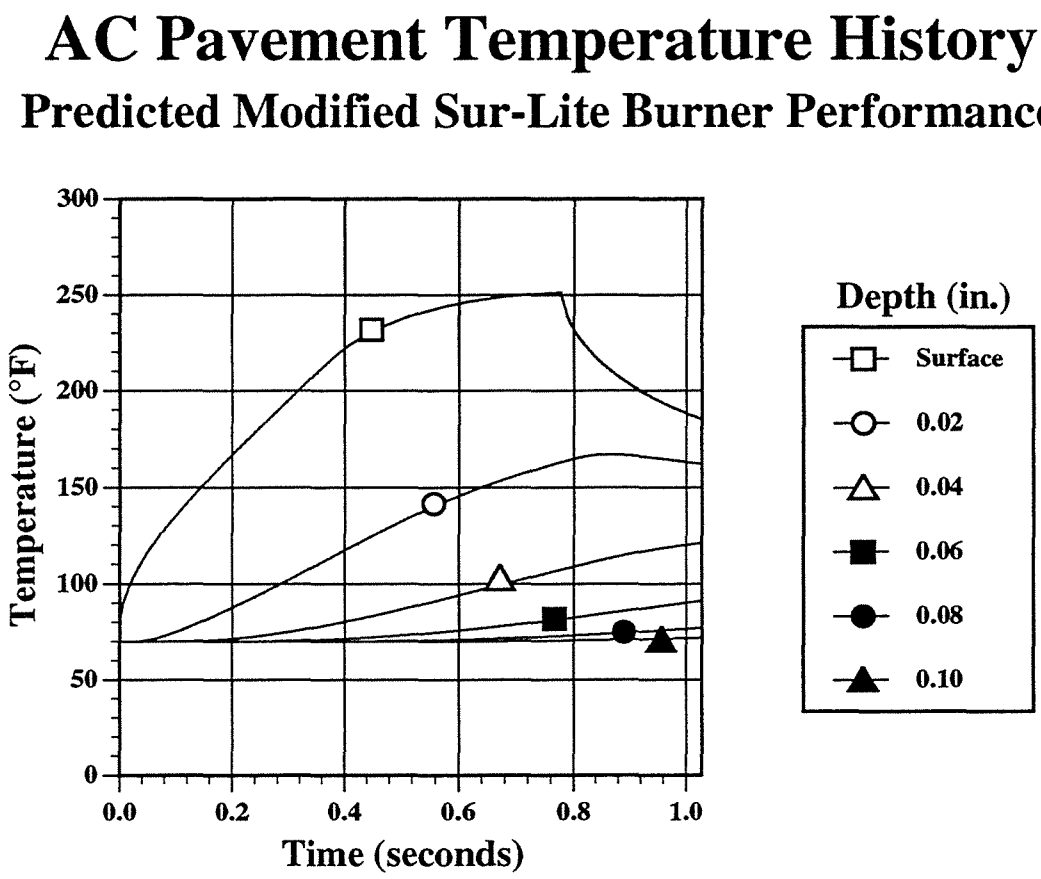

Figure 6.10 - *Predicted modified Sur-Lite burner performance. Relative speed is 2 MPH, nozzle exit diameter is necked down to 3.5", and the exit gas temperature is estimated to be 2000°F.*

6.2.2.4 - Results

Overall, plots of the Sur-Lite burner tests show strong correlation between actual and predicted pavement surface temperature. This can be seen upon quick examination of the plots of the 30 test runs located in the March 1992 interim report. No statistical analysis was performed to quantify this level of correlation however, since any hypothesis formulated would have been based on the assumptions made earlier in the Phase I Final Report, those being: a homogeneous substance structure, a smooth surface texture, a maximum effective convective reach of 4 diameters (r/D_{max}=4) and, negligible air density changes. Also, since only one heater, the Sur-Lite burner, was used in the tests, nothing conclusively, in the strictest sense, can be

stated about the accuracy of the model in simulating other burners. However, for the design aid purpose it was intended, it has been qualitatively proven that the convective model does serve as a sufficient instrument in predicted heater performance.

6.2.3 - Test Conclusions

Based on the tests and simulations performed above, when fitted with a high pressure blower and appropriate fuel train assembly, the Sur-Lite burner does have the potential to adequately serve the needs of this project (see Figure 6.10). As opposed to a radiant heater, the Sur-Lite burner offers compactness and simplicity to the design while achieving a similar end result. And, since most road crews today use an HCA lance as a cleaning and heating method, a similar convective heating method would be more readily accepted by the end user.

Before committing to the Sur-Lite system however, it was felt that because of the physical complexities associated with mounting this burner and blower unit, flame tube, and fuel train on the crack sealing machinery end-effectors, certain design issues should be further discussed. For these reasons outlined in the March 1992 interim report, a trade-off study between various available convective heaters that addresses the design requirements of the heating system was performed prior to final design selection. This resulted in our choice for second generation HCD system integration to purchase and integrate a higher pressure, more compact burner manufactured by Eclipse during Phase III. The system selected therefore, was outlined in detail in the Phase II - Part I Final Report, Section 6.2.

6.3 - Sealant Applicator

6.3.1 - Objective

The objective of the experimental verification of the sealant applicator is to determine the durability of the mounting hardware and various components in a roadway environment. Specifically, the performance of the sealant level monitoring system, the rotating squeegee, the rotating motor including its controller, and the adjustable weight compensation system will be monitored for their reliability. The critical system parameters of the sealant applicator are represented by these components.

6.3.2 - Requirements

The sealant applicator will be judged by the following criteria in Table 6.1.

SQUEEGEE ROT. SPEED	0 TO 80 RPM
OPERATING TEMPERATURE	32 to 400° F (0.0 to 204.4° C)
LEVEL TRANSDUCER ERROR	+/- 5%
WEIGHT COMP. SYSTEM	0 TO 60 LBS
SQUEEGEE WEAR RATE	<1/4" FOR 8 HOURS OPERATION

Table 6.1 - *Sealant Applicator Requirements.*

6.3.3 - Method

A. Set-up

The applicator system test requires the following in Table 6.2.

One sealant applicator assembly
One longitudinal machine with cart
One bridge circuit signal amplifier and modifier
Four strain gauges mounted on the sealant applicator strain ring
Volt meter with mV range of measurement
110 Vac power supply
Pressurized supply of the sealant material

Table 6.2 - *Applicator System Hardware Requirements.*

B. System Connections

Figure 6.11 shows the connections for the sealant level monitoring system. The output of the strain gage amplifier/signal conditioning module correlates with the sealant level in the applicator reservoir. The signal is then fed into a proportional valve which controls the quantity of sealant introduced in the applicator reservoir.

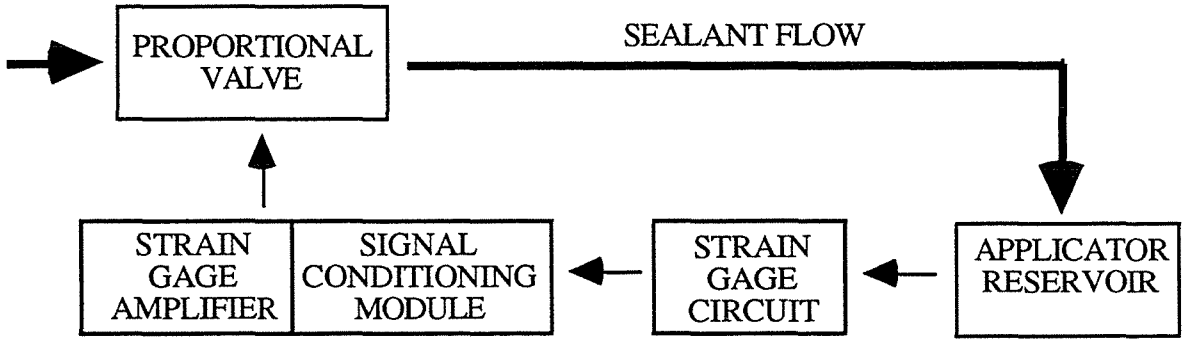

Figure 6.11 - *Sealant Level Monitoring System.*

The weight compensation system connections are illustrated in Figure 6.12. Twin air cylinders support the weight of the sealant applicator so as to reduce wear on the rotating squeegee. Varying the pressure within the static air reservoir varies the force exerted on the applicator assembly by the air cylinders.

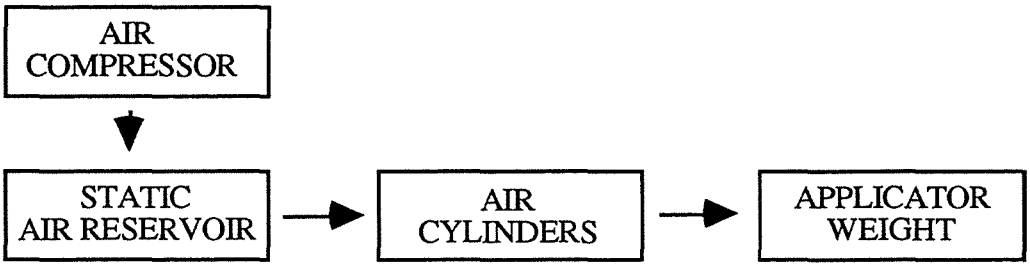

Figure 6.12 - *Weight Compensation System.*

B. Test Procedure

To confirm the performance of the sealant applicator, it will be attached to the longitudinal machine and operated on a road surface at the UC Davis campus. The short duration of the operation will give an initial indication of the reliability and durability of the sealant applicator. Special attention will be given to the critical system components including the rotating squeegee, the rotating motor, and the adjustable weight compensation system. The mounted applicator test assembly is shown in Figure 6.13.

6.3.4 - Results

The sealant applicator successfully sealed both road cracks and prerouted cracks with a flush configuration. The performance of the critical components of the applicator assembly will be crucial to the redesign of the applicator for Phase III.

Rotating Squeegee - Over a four hour period of operation the reinforced nitrile material did not noticeably wear. The sealant buildup on the outside of the ring was only 1/8" thick. Both observations imply that the squeegee is more than sufficient for a day of operation.

Rotating Motor/Controller- Varying the applicator rotational speed improved the quality of the flush configuration. However, the maximum rotational speed of the existing motor was not enough to achieve the optimal flush configuration for a higher truck speed rate. For Phase III it will be necessary to increase the horsepower rating of the

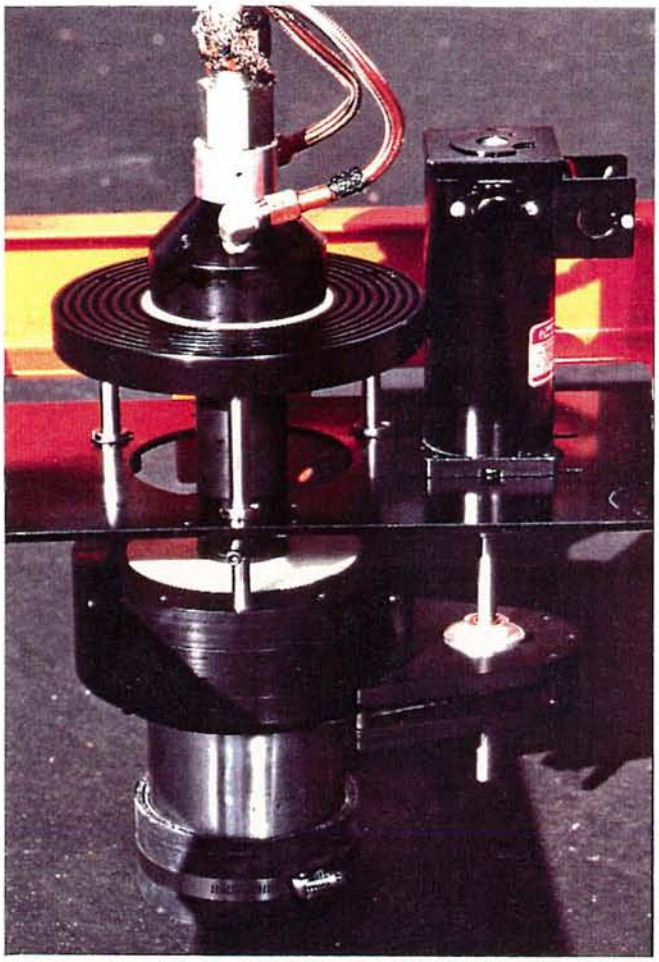

Figure 6.13 - *Sealant Applicator Mounted in Longitudinal Test Cart.*

motor if cracks are to be sealed at a faster rate.

Adjustable Weight Compensation System - The adjusted weight of the sealant applicator with the weight compensation system enabled was approximately 15 lbs. The original weight of the applicator is 55 lbs. Increasing the pressure in the air cylinders, resulted in the loss of free vertical travel. The Thomson shafts would stick in the linear bearings. Briefly introducing high pressure air to the air cylinders pushed the applicator assembly off the roadway in a quarter of a second. This suggested a feature in the Phase III design where the applicator could avoid reflective markers and large debris on the roadway.

Sealant Level Monitoring System - During testing it became apparent that the strain gage circuit would not function in a high temperature, high vibration environment. The leads for the strain gages would break off under continual operation. Only visible flags attached to the floater gave an accurate representation of the amount of sealant in the

sealant reservoir. For Phase III a linear potentiometer/transducer will be attached to the floater in place of the flags. Directly measuring the mechanical travel of the floater will be more accurate than inferring the amount of sealant in the reservoir with the strain gage assembly. In Figure 6.11, the linear potentiometer would replace the strain gage circuit. The signal conditioning module would not have to be modified.

7.0 - VEHICLE ORIENTATION AND CONTROL SYSTEM (VOC)

7.1 - Test Objective

The purpose of the VOC subsystem is to keep track of the vehicle relative to the cracks located by the VSS as the vehicle moves forward, and provide the robot and path-planning subsystems the current location of these cracks. The objective of the stationary and mobile VOC tests was to verify that the VOC hardware and software correctly track position. Critical to the operation of the automated crack sealing machine is the location of cracks on the road surface and the tracking of these cracks as the vehicle moves forward and the cracks come within the robot work space.

7.2. - Requirements

The VOC subsystem keeps track of the moving vehicle's relative position on the road using two optical encoders, a computer and computer software developed to read the encoders, calculate moved positions, and update crack locations relative to a specific new position. A counter card plugged into a standard slot on an IBM compatible computer records the encoder outputs. The VOC performance is determined by the encoders and counter card. The criteria for these components are

ENCODER RESOLUTION (LINES PER REVOLUTION)	2500
MINIMUM DISTANCE RESOLUTION	0.0625" (1.588 mm)
ENCODER OUTPUT	5V
ENCODER SUPPLY VOLTAGE	5Vdc
ENCODER OUTPUT FORMAT	channels A and B
ENCODER CABLES	shield, twisted pair
FIFTH WHEEL RADIUS	8" (203 mm)
TEMPERATURE	0-70 C
HUMIDITY	100% RH
VIBRATION	5-2000 Hz
SHOCK	20G

Table 7.1 - *Encoder Requirements.*

shown in Tables 7.1 and 7.2. The most critical condition is the distance resolution which is determined by the encoder's resolution, and for VOC purposes this must be greater than 0.0625".

MINIMUM NUMBER OF COUNTING CHANNELS	5 up and down channels
BUS COMPLIANCE	IBM compatible bus
COMPUTER	IBM compatible 386-25MHz
MINIMUM INPUT FREQUENCY	2kHz
POWER REQUIREMENTS	5V
TEMPERATURE	0-65 C
HUMIDITY	95% RH
VIBRATION	2.5 G peak acceleration
SHOCK	30G peak acceleration

Table 7.2 - *Counter Card Requirements.*

7.3 - Method

7.3.1 - Setup: Measurement System and Software

The hardware and software shown in Table 7.3 was used to perform the VOC tests. Two incremental pulse encoders were used as the position transducers, and provided information on the vehicle's incremental position and heading. The encoders have a resolution of 2500 pulses per revolution. This results in a position error of 0.02 inches and a heading error of 0.14 degrees per pulse. The Metrabyte CTM05 card has five sixteen-bit counters. One counter is used to generate a periodic sampling interrupt, while the other four are used to record the A and B channel outputs from each encoder. The A and B channels of each encoder output the same frequency pulse with a 90 degree phase shift, and could be used to detect if the vehicle is moving forward or reverse. In the current configuration, only the output of the A channels are used, but in the prototype machine both A and B channels will be used in conjunction with an up and down counter.

The system software consists of a C program with the following major functions:

- the program reads the encoder output recorded by the counter card ten times a second;
- calculates the incremental distance and heading change, and;

- accumulates the incremental distances and headings to compute the current position and heading.

The program flow chart is shown below on Fig. 7.1, and illustrates the relationships of the four main functions.

IBM compatible 386-25 MHz computer
Two incremental pulse encoders
One Metrabyte CTM05 Counter Card
Measurement system software
Test apparatus - mobile cart or stationary platform

Table 7.3 - *Test Hardware & Software.*

The calculated distances reported here are those obtained from this program, and are compared to the distances measured on the shop floor. The encoders output a square wave pulse as they rotate, and the data acquisition card registers the number of pulses transmitted. The computer software reads the number of recorded pulses and then calculates the distance the cart has moved and the cart heading. The distance traveled is calculated in the software using kinematics schemes described below.

7.3.2 - Test Procedures

7.3.2.1 - Measurement Procedure

The algorithms for measuring distance and heading are adopted from a measuring system proposed by Tsumira, et al. (1982)[1] for measuring vehicle position and heading. The procedure consists of the following steps:

1. Compute the distance traveled during one pulse.

$$\frac{2 * \pi * Radius}{Counts\_Per\_Revolution} \tag{7.1}$$

Let D_l and D_r be the distance/pulse for the left and right encoders respectively.

[1]Tsumira, T., N. Fujiwara, T. Shirakwaw and M. Okazaki. Bulletin of the Japanese Society of Mechanical Engineers, Vol 25, No. 203, May 1982.

2. Compute the number of counts recorded during the sampling period.

$$\begin{aligned} N_l &= N_{l2} - N_{l1} \\ N_r &= N_{r2} - N_{r1} \end{aligned} \tag{7.2}$$

3. Compute the distance traveled for each wheel,

$$\begin{aligned} \Delta L_l &= D_l * \mathrm{N}_l \\ \Delta L_r &= D_r * \mathrm{N}_r \end{aligned} \tag{7.3}$$

the incremental distance traveled,

$$\Delta L = \frac{\Delta L_l + \Delta L_r}{2} \tag{7.4}$$

and the incremental heading change.

$$\Delta\theta = \frac{\Delta L_l - \Delta L_r}{Wheel\_Base} \tag{7.5}$$

4. Compute current heading.

$$\theta_n = \theta_o + \Delta\theta \tag{7.6}$$

5. Compute current position.

$$\begin{aligned} X_n &= X_o + \Delta L * COS(\theta_o + \Delta\theta/2) \\ Y_n &= Y_o + \Delta L * \mathrm{SIN}(\theta_o + \Delta\theta/2); \end{aligned} \tag{7.7}$$

where X_o and Y_o are the previous position, θ_o the previous heading, X_n and Y_n are the current position, and θ_n the current heading.

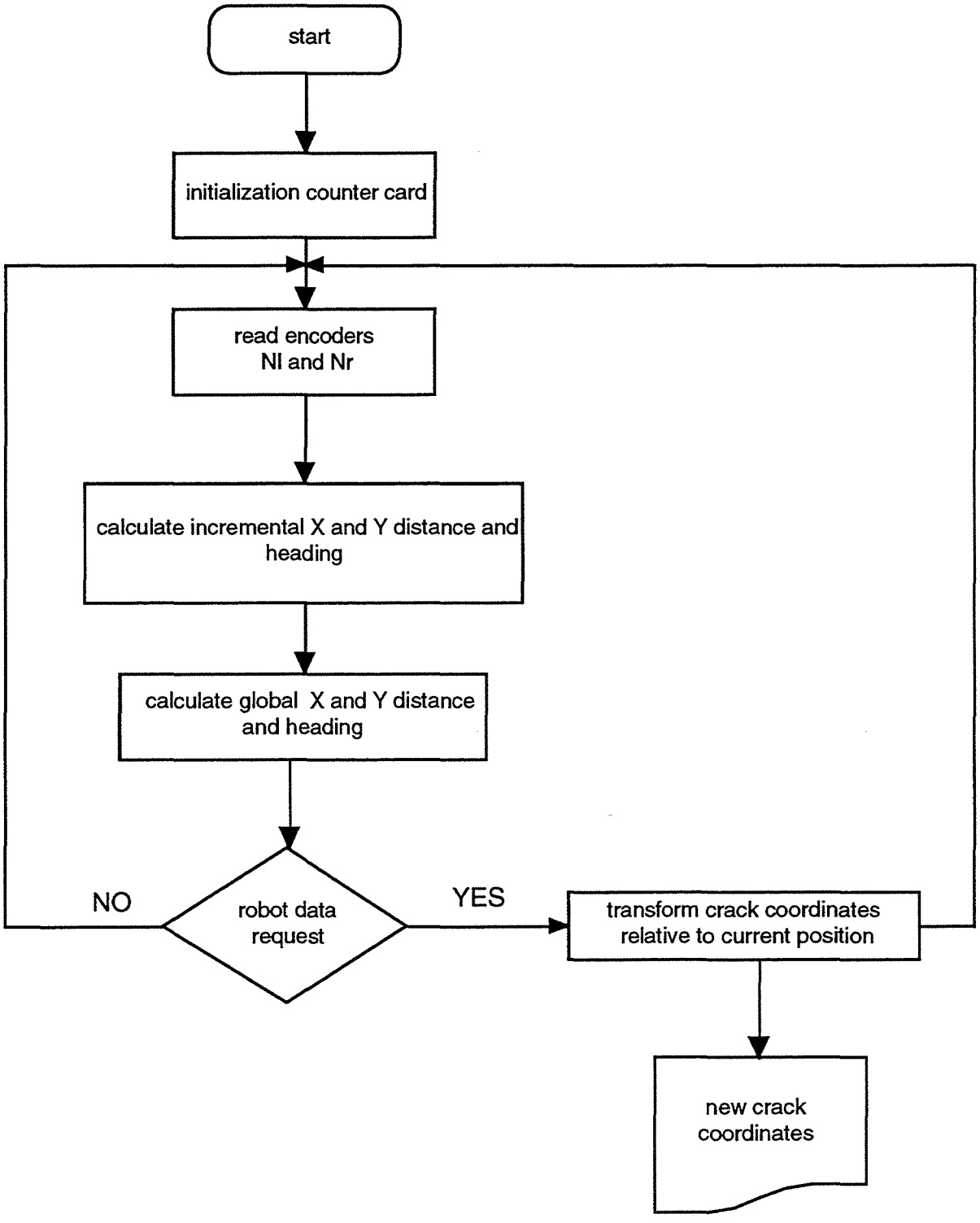

Figure 7.1 *- VOC Program Flow Cart.*

7.3.2.2 - Stationary Test Procedure

In the stationary platform test, the encoders were mechanically attached together and rotated manually or with a variable speed electric motor. This test condition simulated a vehicle traveling along a straight path. The procedure has the following steps:

1. Connect the stationary platform as shown in Figs. 7.2 and 7.3. Fig. 7.3 shows the two encoders, the DC motor, the SCR motor controller and computer.
2. Start the measuring system program.
3. Manually rotate the connecting encoder pulley a known distance. This can also be accomplished by using a motor controlled pulley, and rotating the encoder pulley a know number of revolutions and calculating the distance rotated.
4. Record the measuring system program's calculated distance.
5. Record the known distance and compare it to the calculated distance.

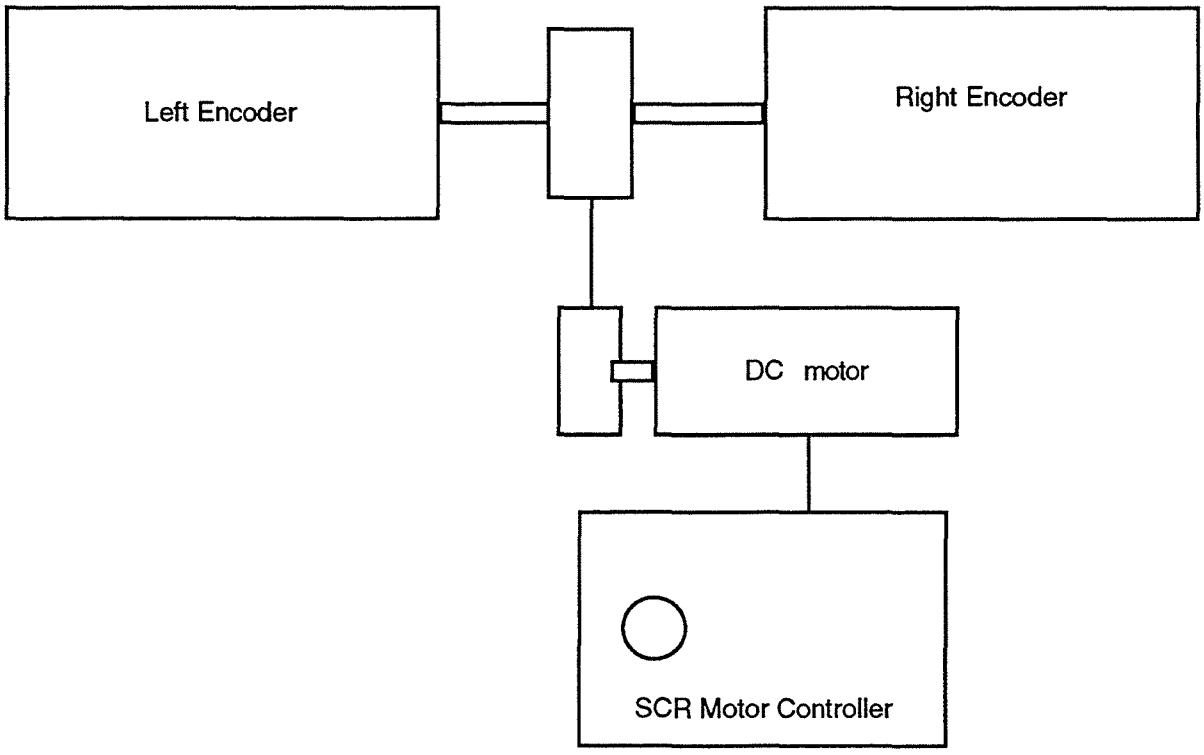

Figure 7.2 *- Stationary Platform Component Schematic.*

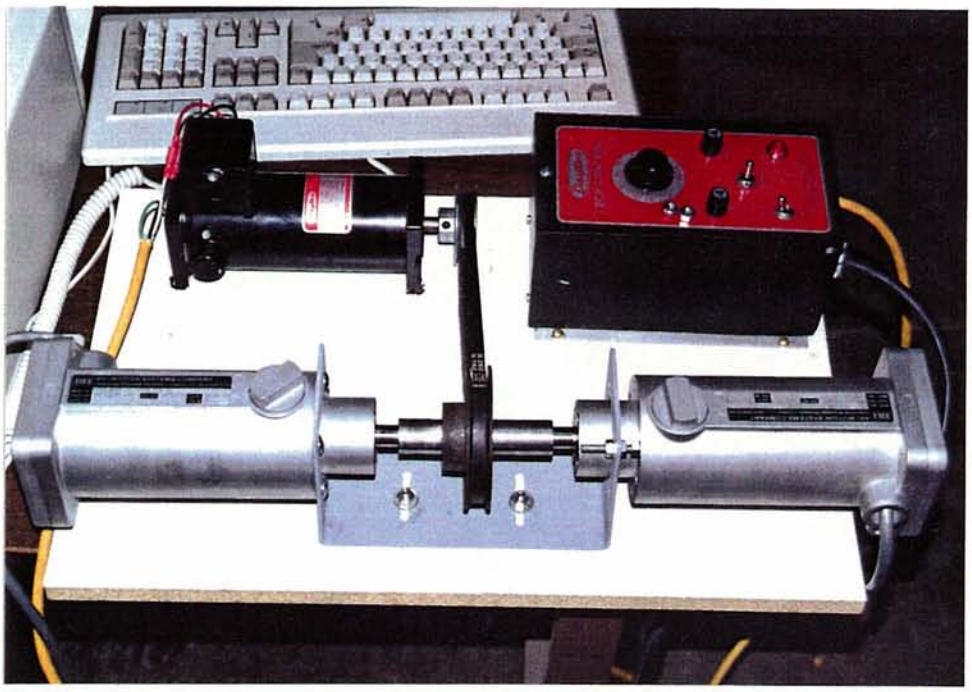

Figure 7.3 - *Photograph of Stationary Platform Test Components.*

7.3.2.3 - Mobile Cart Test Procedure

The mobile cart had the two encoders attached to the back, non-steering wheels and was pulled on a concrete shop floor as the computer recorded the encoder output. Several paths were followed and the calculated distances compared to measured floor distances. The procedure consists of the following steps:

1. Connect the hardware as shown in Fig. 7.4.
2. Mark on the shop floor the middle point of the rear axle to indicate the starting position.
3. Start the measuring system program.
4. Pull the cart along a random path for about 200 inches.
5. Mark on the shop floor the middle point of the rear axle to indicate the end position.
6. Measure and record the floor distance between the start and end positions.
7. Record the measuring system program's calculated distance and compare that to the distance measured on the floor.

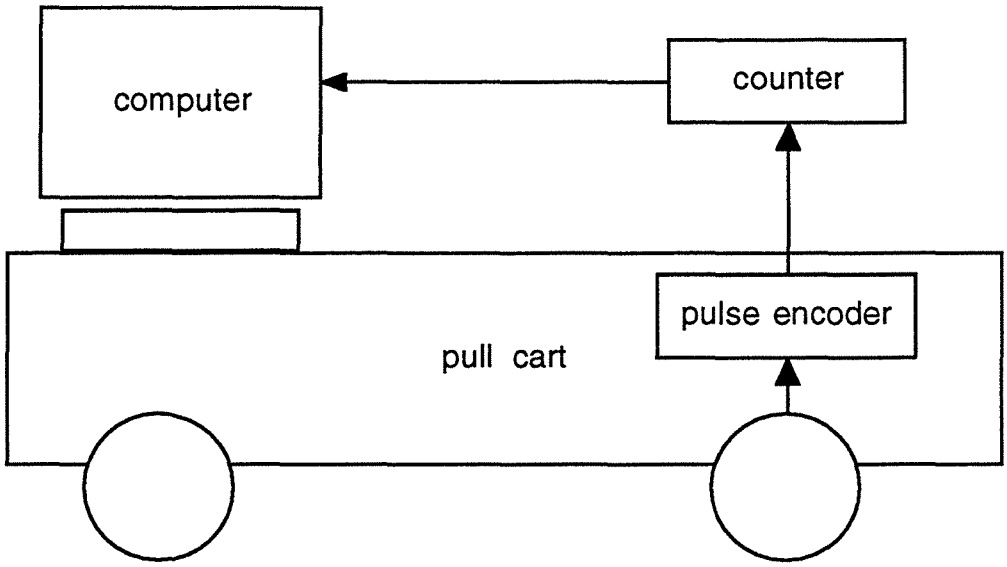

Figure 7.4 *- Mobile Test Cart Component Schematic.*

7.4 - Test Results

7.4.1 - Stationary Platform Test Data

The data shown in Table 7.4 is the cumulative summary of ten repetitions of the stationary platform tests. The X-distance reflects the number of revolutions the encoder pulley wheel turned, and the error is the cumulative deviation recorded over the run. Figure 7.5 is a plot of the X-distance rotated compared to the cumulative error.

Table 7.5 is a detailed log of one test run, and shows the incremental changes. Under the stationary platform test conditions both the encoder and distance errors should be zero.

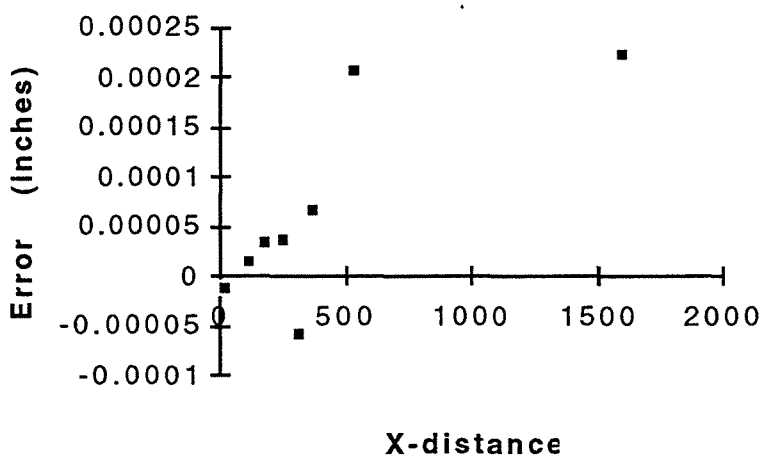

Figure 7.5 *- Plot of the Straight Line Encoder Test Runs.*

Test Run	Left Encoder	Right Encoder	Encoder Error	X-distance (inches)	Error (inches)
1	9301	9301	0	376.171791	0.000065
2	35324	35323	1	177.555277	0.000031
3	5344	5342	2	191.551701	0.000031
4	41836	41835	1	539.708025	0.000207
5	35105	35105	0	176.456976	0.000034
6	3536	3538	-2	17.778901	-0.000012
7	50742	50741	1	255.054598	0.000035
8	22831	22831	0	1597.15052	0.000222
9	63448	63449	-1	318.926946	-0.000059
10	22048	22047	1	110.822822	0.000015

Table 7.4 - *Results of the Straight Line Encoder Tests.*

7.4.2 - Mobile Cart Test Data

The data in Table 7.6 shows the cumulative summary of eight mobile cart tests. The measured distance is compared with the distance calculated using the VOC hardware and software. Figure 7.6 is a plot comparison of this same data. The paths followed for these test runs were random.

7.5 - Discussion

7.5.1 - Stationary Test Discussion

The objective of the stationary tests was to verify the operation of the encoders, counter card, and software without the dynamics of any road interactions. Figure 7.5 and Table 7.5 show that the distance error accumulates the further the vehicle travels. The maximum error on the stationary platform was 0.00004 percent and was recorded for a test run over 540 inches. This is an insignificant error. An encoder error of one pulse can be expected because with the current counter card, pulses are not latched simultaneously, and small deviations will occur especially at high pulse frequencies.

Additional errors will occur if the encoders are not aligned correctly. While this was a source of significant errors in earlier tests, the current results demonstrate that this is no longer a problem.

Sample	Left Encoder	Right Encoder	Encoder Error	X-distance (inches)	Error (inches)
0	3	3	0	1.141026	0
1	230	230	1	2.385097	0
2	478	477	0	5.66492	0.000001
3	1130	1130	0	7.600141	0.000001
4	1515	1515	0	12.20446	0.000001
5	2431	2431	1	14.76549	0.000001
6	2941	2940	0	19.49798	0.000002
7	3882	3882	0	21.53373	0.000002
8	4287	4287	1	86.17766	0.000013
9	49916	49915	1	87.98219	0.000013
10	50275	50274	0	91.06095	0.000014
11	50887	50887	1	92.48597	0.000014
12	51171	51170	0	95.44913	0.000014
13	51760	51760	0	96.99228	0.000014
14	52067	52067	0	100.3048	0.000014
15	52726	52726	0	102.0088	0.000014
16	53065	53065	0	105.3213	0.000014
17	53724	53724	1	106.8418	0.000015
18	54027	54026	1	109.8125	0.000016
19	54618	54617	0	111.2275	0.000016
20	54899	54899	0	114.3791	0.000016
21	55526	55526	0	116.0328	0.000016
22	55855	55855	0	119.4559	0.000016
23	56536	56536	1	121.087	0.000016
24	56861	56860	1	124.1482	0.000017
25	57470	57469	1	125.5858	0.000018

Table 7.5 - *Sample Data Collected During a Test Run.*

Test Run	Measured distance	Calculated distance	Error
1	168.5	168.5	0
2	185.6	185.4	0.2
3	164.8	164.8	0
4	173.9	174.1	-0.2
5	195.5	198.6	-3.1
6	186.4	188.3	-1.9
7	180.2	180.9	-0.7
8	196.2	197.7	-1.5

Table 7.6 - *VOC Cart Test Data.*

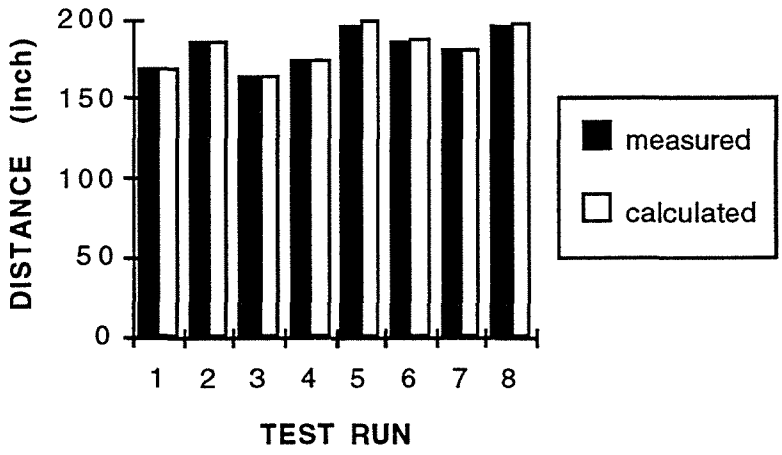

Figure 7.6 - *Results of VOC Cart Tests.*

7.5.2 - Mobile Test Discussion

The results of eight test runs are attached. Five runs were along relatively straight paths (1, 2, 3, 4 and 7) and three along curved paths (5, 6 and 8). Figure 7.7 is a path plot of a straight path, which for the mobile test cart means that the middle of the cart's rear axle is never greater that four inches laterally displaced (Y-axis direction) from the starting position. Similarly, Fig. 7.8 is a path plot of a curved path, which means that the middle of the cart's rear axle is displaced greater that four inches laterally from the starting position during its motion. The correlation between the measured and calculated positions for paths that are relatively straight (runs 1, 2, 3 and 4) have a

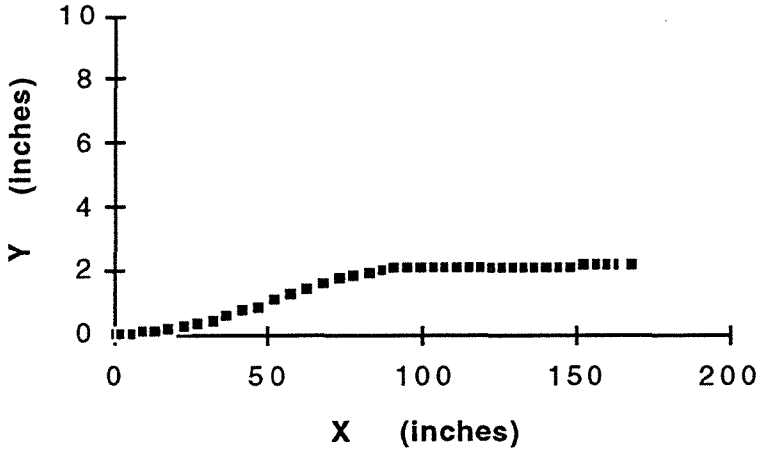

***Figure 7.7** - X-Y Path for Run 1.*

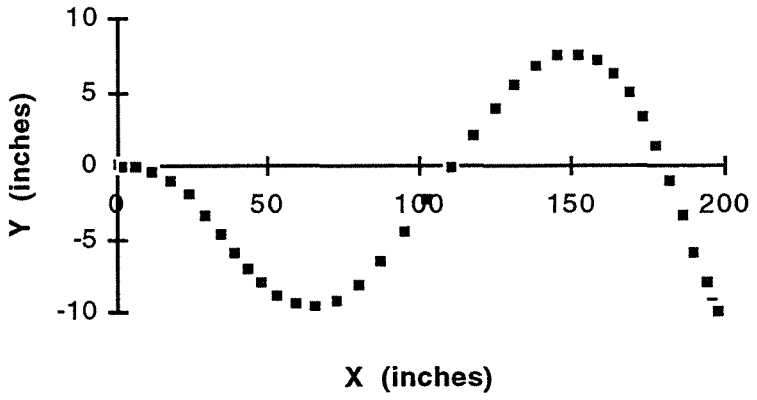

***Figure 7.8** - X-Y Path for Run 5.*

deviation of less than 0.01 percent, and these measured distances are within the measurement error limits of the measuring tape. Results for paths that are curved have deviations greater than 0.01 percent and result in errors greater than one inch over forty feet (runs 5, 6 and 8).

Three types of errors were identified from these tests. The first type of error is due to electrical-mechanical noise and results in spurious counts. The spurious counts indicate that the encoders have rotated a larger or smaller distance than is the case. Reducing this error has been the focus of most of the work to date. This error has been reduced, and as shown in the test results may not be a significant source of inaccuracies.

The second type of error is due to the resolution. Using the current encoder, we can resolve a rotation of up to 0.08 degrees. The true rotation is within this margin. With lower resolution encoders, we resolve larger angles, and thus have a larger error. For purposes of the VOC, this error is not expected to be significant because cracks are tracked for forty foot sections, and the accumulation of the errors is less than the crack resolution.

The third type of error is due to the interaction of the cart wheels and the floor surface. This error includes changes in wheel radius and wheel base, and wheel slip as the cart moves along the floor. In our current test setup, this type of error is the most significant and may account for the errors resulting from following a curved path such as run 5. To illustrate, a wheel radius change of 0.04 inches over a 165 inch run results in a deviation of 1.6 inches. Control of this source of error will be handled in the fifth wheel prototype by having a rigid wheel base and hard rubber tires that reduce the wheel radius deviations.

7.6 - Conclusions

The test results for the stationary platform demonstrated that there are no significant measurement errors, and verify that the encoders, the counter card and software all are functioning correctly.

The mobile cart test results demonstrated that the hardware and software provide position data within the measurement limit for straight paths, but require additional hardware modification to control errors when following curved paths. The hardware modifications will be made in the prototype fifth wheel design, and additional mobile cart tests will be performed to ensure the proper functioning of the VOC hardware.